THESIS

ASSESSING THE IMPACTS OF CLOUD CONDENSATION NUCLEI ON CUMULUS CONGESTUS CLOUDS USING A CLOUD RESOLVING MODEL

Submitted by

Amanda M. Sheffield

Department of Atmospheric Science

In partial fulfillment of the requirements

For the Degree of Master of Science

Colorado State University

Fort Collins, Colorado

Fall 2011

Master's Committee

Advisor: Susan C. van den Heever

Sonia Kreidenweis
Richard Eykholt

ABSTRACT

ASSESSING THE IMPACTS OF CLOUD CONDENSATION NUCLEI ON CUMULUS CONGESTUS CLOUDS USING A CLOUD RESOLVING MODEL

Cumulus congestus clouds are mid-level clouds that form part of the trimodal tropical cloud distribution. They act to moisten the atmosphere and may become mixed-phase in their lifetime. Congestus typically surpass the tropical trade wind inversion from where they may either develop into deeper convection, or alternatively remain as terminal congestus. Such growth is dependent on multiple factors, including those which alter the local environment and the microphysical structure of the cloud. This study investigates the impacts of cloud condensation nuclei (CCN) on cumulus congestus clouds through the use of large domain, cloud-resolving model (CRM) simulations in radiative convective equilibrium (RCE). Previous studies have focused on the convective invigoration of congestus and their subsequent growth to deep convection in association with ice processes. This study will focus on the response of congestus clouds to more polluted conditions, with particular emphasis on the development and growth of congestus from the warm phase to beyond the freezing level.

It is found that convection is invigorated in the more polluted cases in association with the enhanced latent heat released during the vapor diffusional

growth of cloud droplets in the warm phase. Such invigoration results in stronger updraft speeds, enhanced vertical lofting of cloud water, and a subsequent increase in the number of clouds growing to above the freezing level. The lofted cloud water is available to form more ice, however the ice water produced is smaller in magnitude compared to cloud water amounts above the freezing level. The low amounts of ice result in relatively insignificant contributions of the latent heat of freezing to the updraft strength. The impacts of enhanced CCN concentrations on various other cloud characteristics and microphysical processes are also investigated.

ACKNOWLEDGEMENTS

I would like to acknowledge those that helped produce this work, including my advisor Dr. Sue van den Heever, the students and research staff of the van den Heever research group and the atmospheric science department, and my husband, Jesse, who is always there to encourage me. This work was supported by two fellowships during my master's tenure in addition to National Science Foundation Grant ATM-0820557, including the American Meteorological Society First Year Graduate Fellowship (2009-2010) and the Department of Energy (DOE) Office of Science Graduate Fellowship (SCGF) (2010 – present). Lastly, I would like to thank my masters committee, Sue, Dr. Sonia Kreidenweis and Dr. Richard Eykholt, for their review of this thesis and its results.

TABLE OF CONTENTS

1. INTRODUCTION

The presence of clouds is important to our understanding of the climate system, as they serve as integral parts of the radiative and hydrologic systems (Solomon et al. 2007). Of interest to this study is a convective cloud type that forms part of the tropical cloud regime (Johnson et al. 1999): the cumulus congestus cloud. The formation of convective clouds and precipitation is dependent on ambient environmental characteristics. These large regional to global scale factors affect a cloud's vertical and horizontal development, size and thickness, updraft speed, and precipitation. However, various microphysical factors may also influence cloud characteristics, including the impact of aerosols on the thermodynamic and dynamic structure of clouds. The goal of this study is to examine the impacts of ambient aerosol concentrations on these cloud characteristics from a large sample of cumulus congestus clouds, including the production of cloud water and ice and contributions to convective invigoration. This goal is to be achieved using a series of idealized radiative convective equilibrium (RCE) simulations of tropical oceanic clouds under the influence of an aerosol layer of varying number concentrations.

Cumulus congestus clouds are defined as "a strongly sprouting cumulus species with generally sharp outlines and, sometimes, with a great vertical development; it is characterized by its cauliflower or tower aspect, of large size." (American Meteorology Society Glossary 2011). These mid-level clouds supply

moisture to the middle troposphere as they evolve from trade wind cumulus clouds and may transition into deep convection. They frequently reach the freezing level and above. As part of the trimodal distribution of clouds commonly observed in the tropics (Johnson et al. 1999), understanding these clouds is important to understanding the overall sensitivity of the development of tropical convective clouds to aerosol indirect effects.

Evaluation of aerosol impacts on cumulus congestus clouds will allow a better understanding of their mixed-phase growth. These clouds commonly reach the freezing level of the atmosphere and subsequently become mixed-phase systems. Such growth may be enhanced through convective invigoration in association with the development of cloud water and ice (Andreae et al. 2004), but may be reduced by the stable layer formed in association with the freezing level (theorized to be formed by subsidence and melting in the tropics) (Johnson et al. 1999, Posselt et al. 2008). The aerosol-congestus cloud interaction may alter these enhancing and reducing factors.

An aspect influential in cloud and ice formation processes is the presence of cloud condensation nuclei (CCN). It has been hypothesized (Twomey 1974, 1977, Albrecht 1989) and observed (Andreae et al. 2004, Rosenfeld 1999) that in more polluted scenarios increased CCN concentrations lead to greater cloud water mixing ratios and the suppression of rain formation processes. Increased cloud water allows for the increased availability of supercooled cloud water aloft (Khain et al. 2005 and others). This supercooled water is then available to freeze, through

nucleation or riming, releasing latent heat, and thus allowing additional convective invigoration.

Convective invigoration through the creation of cloud water and ice are not the only effects taken into account in cloud dynamics. Aerosols may also influence cold pool development and condensate loading. Cold pools have been found to be weaker in more polluted scenarios (Storer et al. 2010), resulting in altered subsequent dynamical development. In more polluted scenarios, condensate loading may increase due to the aerosol induced increased water and ice mass within the cloud. Evaluation of these effects with varying concentrations of aerosol that can serve as CCN will also be investigated.

The modeling experiment presented here includes a field of tropical convection in RCE that is impacted by a layer of aerosols acting as CCN. This idealized aerosol experiment is similar to tropical oceans impacted by dust layers, such as the Saharan Aerosol Layer over the Atlantic Ocean and Gulf (Prospero 1999). In this study, we will investigate the effects of CCN on the cloud microphysics and dynamics of cumulus congestus clouds developing within a field of tropical convection. Chapter 2 provides a background of this study, followed by a discussion of the method (chapter 3). Chapter 4 is the results of this investigation, including discussion. Concluding remarks are in chapter 5.

2. BACKGROUND

2.1 THE IMPORTANCE OF CLOUDS

Clouds are intriguing, complex phenomena that are important to our understanding of the hydrological cycle and the radiation balance of the Earth. In-situ methods and numerical models have been used to study them, but the lack of a complete understanding of clouds leaves current global climate predictions at a disadvantage. The presence of clouds may play a major role in climate change (Houghton et al. 2001, Ramanathan et al. 2001, Arakawa 2004, Stephens 2005). The most recent Intergovernmental Panel on Climate Change (IPCC) report discussed the deficit in our knowledge of cloud-aerosol interactions and the un-quantified impacts on climate (Solomon et al. 2007). In addition to aerosol interactions, aspects such as cloud type, life cycle, ambient environment, and water phase complicate clouds. Any thermodynamic or dynamic factor impacting these characteristics and the overall life cycle of the cloud is vital to understanding climate change questions.

2.2 CLOUD NUCLEI AND THEIR EFFECTS

Discovery of the impact of cloud nuclei on cloud microstructure occurred in early studies comparing maritime- and continental-sourced cumuli (Squires 1956, 1958). Maritime cumuli were found to contain a lower concentration of larger radii cloud droplets than comparable continental cumuli, which were found to contain a

relatively larger concentration of smaller radii cloud droplets (figures 2.1 and 2.2). These original studies were focused on warm rain cumuli. A key to understanding this difference was the presence of cloud-nucleating aerosol in the cloud formation process. These aerosols can serve as cloud or ice nuclei, and have been linked experimentally to cloud droplet and ice formation (Squires and Twomey 1960, Twomey and Warner 1967). A cloud droplet or ice particle forms on a cloud or ice nucleus due to water or ice supersaturated conditions found in a cloudy parcel. A cloud droplet cannot form without a cloud condensation nucleus in conditions found on Earth (Pruppacher and Klett, 1997). Ice may form with or without an ice nucleus, but may be altered by their presence.

Continental air masses commonly contain higher aerosol concentrations produced by anthropogenic (such as soot) and natural (such as dust) sources. Maritime air masses may lack these land-based aerosols due to distance from the source, but do have greater opportunity for oceanic sources of aerosol, such as sea salt. Trying to understand the relationship between aerosols and cloud formation has led to several proposed indirect effects.

The aforementioned studies established the link between cloud and ice nuclei and cloud droplet and ice formation. However, the overall impacts of this link are yet to be fully understood. Several aerosol-cloud interaction theories have been proposed and confirmed by observations in the last four decades following these discoveries, but our complete understanding and quantification is yet in progress. Theories suggesting that ambient aerosol concentration could impact clouds are called aerosol indirect effects (AIEs). The first AIE (Twomey 1974, 1977) suggests

that for the same liquid water content, an increase in cloud droplet number concentrations and subsequent decrease in cloud droplet size in the presence of a given number of aerosols that are able to serve as CCN results in an increase in the cloud albedo. The second AIE, or cloud lifetime effect (Albrecht 1989), extends this thought by suggesting that a decrease in cloud droplet size reduces drizzle in stratocumulus and fair weather cumulus clouds, thereby increasing the clouds' lifetime. These AIEs appear to be greatest where background aerosol concentrations are low (van den Heever and Cotton, 2007). Change in cloud properties will affect liquid water content, fractional cloudiness, and the albedo of the cloud in comparison with the surface (Lohmann et al. 2005). One such example is a characteristically clean atmosphere over an ocean. A more polluted atmosphere could increase the cloud fraction over that region of the ocean, thereby impacting the albedo of that region due to the higher albedo of clouds compared to the surface.

Cloud nucleating particles are classified as cloud condensation nuclei (CCN), ice nuclei (IN), or giant CCN (GCCN) (Pruppacher and Klett, 1997). CCN are aerosol particles capable of activating cloud droplet formation through heterogeneous nucleation. CCN concentrations (at approximately 0.1 to 1% supersaturation) are commonly found to be a few hundred per cm^3 over the oceans (Pruppacher and Klett, 1997) and a few hundred to a few thousand per cm^3 over continents, though these values can vary by region and source. CCN are more abundant than other cloud and ice nucleating particles, such as GCCN and IN. GCCN are CCN of larger sizes that can more readily form cloud droplets through activation of larger haze particles but lack sizeable concentrations and have a large settling velocity. IN are

aerosol particles capable of activating ice particles at temperatures below freezing through heterogeneous nucleation. The nucleating abilities of each type of nucleus affects the AIEs mentioned above plus mixed- and ice phase processes and cloud properties, such as local supersaturation.

2.3 DUST AS CLOUD NUCLEI

There are many natural and anthropogenic sources of aerosols, including dust from deserts, smoke from biomass burning, and air pollution. Important to the understanding of the aerosol representation in this study is the role of dust as CCN. Dust is transported on regional and global scales. Examples of this include transport from East Asia over the Pacific and observed as far as the western US (Sassen 2002) and transport from North Africa (the Sahara and the Sahel) over the subtropical Atlantic (Prospero 1999). Recent studies of an Atlantic dust event during the CRYSTAL-FACE (Cirrus Regional Study of Tropical Anvils and Cirrus Layers – Florida Area Cirrus Experiment) field campaign showed that dust residue from a Saharan Air Layer (SAL) resided at 1 - 4 km in altitude over Florida (Demott et al. 2003, Sassen et al. 2003, Cziczo et al. 2004, Prenni et al. 2007). Samples collected from western Africa and the eastern Atlantic Ocean during the NAMMA (NASA African Monsoon Multidisciplinary Activities) experiment found higher than expected cloud droplet number concentrations for characteristically clean Atlantic maritime clouds (Twohy et al. 2009). These higher than expected cloud droplet number concentration clouds occurred in regions of high crustal particle dust (figure 2.3b) and the observed clouds contained this crustal material (figure 2.3a) (Twohy et al. 2009). These dust particles are able to serve as IN (Demott et al. 2003,

Twohy et al. 2005) and CCN (Twohy et al. 2009). Dust samples compared between Asian and Saharan sources have also been found to have similar nucleation behavior (Field et al. 2006), indicating the impacts of dust as cloud-active aerosol to be globally important.

2.4 TRIMODAL TROPICAL CLOUD DISTRIBUTION AND CUMULUS CONGESTUS CLOUDS

Convection in the tropics has been recognized as an important source of atmospheric heat transport (Riehl and Malkus 1958, Malkus 1963). Early studies found that trade wind cumulus clouds play a role in pre-moistening the atmosphere prior to deep convection, and in turn aids in the transport of heat and moisture to the upper troposphere. The study of the distribution of tropical convection in the last 15 years has re-emphasized the importance of the middle, cumulus congestus mode (Johnson et al. 1999). This mode is important to transporting sensible and latent heat throughout the mid-level troposphere and possibly in the transition from shallow to deep convection (Jensen and Del Genio 2006, Luo et al. 2009). Layers of increased static stability in the atmosphere result in the trimodal stratification of tropical convection. These three stable layers also include three separate overturning circulations associated with ascent in convective regions and subsidence in nearby non-convective regions (Posselt et al. 2008).

The cumulus congestus mode occurs at or near the stable layer present near the 0^{o}C level in the tropics (Johnson et al. 1996, 1999), typically occurring around 5 km in altitude. This layer is theorized to be weakly stable and forms through the melting of ice hydrometeors from dissipating anvils, leaving a cooler layer below the

freezing level, or through subsidence, which results in a warmer layer above the freezing level (Posselt et al. 2008, van den Heever et al. 2011). Johnson et al. (1999) renewed interest in observed, western Pacific cumulus congestus clouds. These congestus were observed as tall as 4.5 to 9.5 km above ground level (AGL) and were found to compose nearly half of the convective clouds and one-quarter of the convective rainfall in the western Pacific warm pool, playing a significant role in moistening the middle troposphere. Jensen and Del Genio (2006) found cumulus congestus clouds to occur with cloud bases below 2 km and cloud tops from 3 to 9 km at an ARM site at Nauru Island in the tropical west pacific (figure 2.4).

Jensen and Del Genio (2006) observed that cumulus congestus clouds contribute a significant portion of the western Pacific precipitation, and congestus have also been found to contribute a significant fraction of the total number of precipitating, tropical clouds (Haynes and Stephens 2007, figures 2.5 and 2.6). As seen using CloudSat satellite data, cumulus congestus clouds contribute most to precipitation in the western Pacific compared to other tropical oceans (figures 2.6 and 2.7), but have comparable contributions to the frequency of precipitating clouds as shallow and deep convection in other regions.

Observational and parcel model studies have found that relative humidity in the mid-levels is a controlling factor in determining cumulus congestus cloud development, more important than the stable layer found near the freezing level (Redelsperger et al. 2002, Takemi et al. 2004, Jensen and Del Genio 2006). However, in a scenario such as assumed in this work, where convective region relative humidity is less varying than those studies, we are able to evaluate the

ability of cumulus congestus clouds to grow vertically beyond the freezing level due to aerosol perturbations. The supply of latent heat both from warm and cold cloud processes may increase updraft buoyancy and cloud invigoration, thus improving the cloud's development to deeper convection. Using CloudSat and MODIS satellite data, Luo et al. (2009) found that 30 to 40% of congestus clouds are transient, or still developing vertically due to buoyancy forcing. The rest of the population is terminal, or neutrally or negatively buoyant.

Figure 2.8 has been provided to show a theoretical schematic of the trimodal distribution of clouds, including the cumulus congestus mode (Johnson et al. 1999). Similar to results found in the Regional Atmospheric Modeling System (RAMS) RCE simulations of Posselt et al. (2008), van den Heever et al. (2011), and others, circulations develop in association with rising, convective motion and compensating subsidence. This subsidence, combined with the melting of falling anvil hydrometeors, may result in the stable layer located at the freezing level (Johnson et al. 1999) in addition to the trade and tropopause inversions. The three modes of convection, limited by these stable layers, presented in the Tropics are evident in figure 2.8. These include the convection limited by the trade inversion at approximately 2 km, cumulus congestus convection limited near the freezing level at approximately 4.5 to 5 km, and deep convection limited by the tropopause height at approximately 16 km. The freezing level is hypothesized to vary slightly in height in disturbed (large scale uplift) versus undisturbed regions (large scale subsidence) (Johnson et al. 1999, van den Heever et al. 2011). Detrainment of convection exists at the stable layers, as is seen in these model simulations.

2.5 RELEVANT STUDIES

In a series of studies from 1985 to 1994 (Hobbs and Rangno 1985, Rangno and Hobbs 1991, 1994), Rangno and Hobbs hypothesized several ice formation initiation processes from their observations of maritime and continental cumulus. In modest cumulus clouds (updraft speeds less than 5 to 10 m s^{-1}), they found that most ice particles originate at cloud top once a threshold diameter is reached in droplet size, creating a few ice particles per liter (figure 2.9). These cloud drops had grown by condensation and at cloud top maximum height they are able to heterogeneously nucleate, possibly by contact nucleation, to ice. Once formed, they grew by vapor diffusion at the expense of other droplets (Wegner-Bergeron-Findeisen Process). This growth causes older turrets of cumulus clouds to have higher ice water content but lower liquid water content.

Mixed-phase clouds represent the possibility of aerosol influenced ice formation based on initial changes to the warm phase. Previous modeling studies have tried to evaluate the impact of aerosols on convection. This includes the thermodynamic effect (TE) (Khain et al. 2005, van den Heever et al. 2006). The TE postulates that the smaller cloud droplets resulting from increased aerosols reduce the production of raindrops (observed in Rosenfeld 1999 and Andreae et al. 2004). The smaller cloud droplets remain longer in the cloud and may be lofted above the freezing level and made available to freeze in a mixed-phase cloud, which upon freezing release latent heat and generate more vigorous convection. This may or may not lead to a decrease in precipitation. van den Heever et al. (2006) found stronger updrafts due to latent heat release from freezing of supercooled droplets

with increased aerosols, but surface rainfall, ice production, and subsequent dynamical and microphysical effects were dependent on the type of aerosol present (CCN, IN, GCCN). Seifert and Beheng (2006), Khain et al. (2008), and Khain (2009) found dependence on the cloud type and environment examined and the importance of latent heat of freezing associated with ice. van den Heever et al. (2011) found trimodal specific changes due to varying CCN concentrations (for cumulus congestus clouds, cloud frequency variations as large as 51% and precipitation variations as large as 19%).

This study uses similar methods to the studies mentioned above to investigate the convective invigoration associated with latent heat release from warm and cold hydrometeor formation processes in cumulus congestus clouds by aerosols. Latent heating sources include nucleation of cloud droplets and ice, condensation onto cloud droplets and deposition onto ice due to vapor diffusion, and riming by hydrometeors. Also presented are some of the processes that comprise the w-momentum equation in addition to latent heating. The w-momentum equation is derived below.

2.6 THE W-MOMENTUM EQUATION

Of importance to this investigation of the convective invigoration of cumulus congestus clouds is a discussion of the w-momentum equation. This equation includes forcing on the updraft speed in association with vertical changes in pressure, frictional forces in the vertical, and buoyancy due to temperature changes and condensate loading. It is the buoyancy term that is of particular importance to

this study because of the influences of condensate formation on latent heat release, and thus cloud temperature, and condensate loading.

Beginning with the Cartesian coordinate form of the w-momentum (equation 1), the three terms on the right hand side are gravity, the vertical pressure gradient term, and the vertical friction term. The vertical friction term has been labeled as F_{rz}.

$$\frac{dw}{dt} = -g - \frac{1}{\rho}\frac{\partial p}{\partial z} + F_{r_z} \tag{1}$$

In the following derivation the ambient environmental variables will be labeled with a $\overline{(\ )}$ while those related to an air parcel will carry no superscripts. Following Holton (2004) and using the assumption that the pressure of the air parcel instantaneously adjusts to that of the environment after lifting $\left(p = \overline{p}\right)$ and the hydrostatic balance assumption for the ambient environment, results in equation (2). This equation now contains a parcel buoyancy term (currently not including condensate drag), a vertical pressure gradient term, and a vertical friction term on the right hand side.

$$\frac{dw}{dt} = -g\left(\frac{\rho - \overline{\rho}}{\rho}\right) - \frac{1}{\rho}\frac{\partial\left(p - \overline{p}\right)}{\partial z} + F_{r_z} \tag{2}$$

The term of importance to this study is the parcel buoyancy term. This is due to the effects of aerosol on this term as a result of changes in temperature via latent heating. Simplifying the first term on the right hand side in equation (2) using the equation of state and the definitions of T_v and θ_v (equation 3) and correcting for condensate drag (r_{cond}), produces the form of the w-momentum equation shown in

equation 4. This equation shows that the updraft speed is a function of the difference between the virtual potential temperature of the environment and the air parcel, any condensate present, the vertical pressure gradient, and the vertical friction term. This study will be referring to the parcel buoyancy term, corrected for condensate, as BUOY and is defined in equation 5.

$$-\left(\frac{\rho-\overline{\rho}}{\rho}\right)=-\left(\frac{p\overline{T_v}-\overline{p}T_v}{p\overline{T_v}}\right)\approx\frac{\theta_v-\overline{\theta_v}}{\theta_v} \tag{3}$$

$$\frac{dw}{dt}=g\left[\left(\frac{\theta_v-\overline{\theta_v}}{\overline{\theta}_v}\right)-r_{cond}\right]-\frac{1}{\rho}\frac{\partial\left(p-\overline{p}\right)}{\partial z}-F_{r_z} \tag{4}$$

$$BUOY=g\left[\left(\frac{\theta_v-\overline{\theta_v}}{\overline{\theta}_v}\right)-r_{cond}\right] \tag{5}$$

Equation 4 defined the three processes that can affect the local time rate of change of updraft speed. These included changes in BUOY, the vertical pressure gradient, and friction. Friction has been assumed to be small (Holton 2004). In this study it will be highlighted that impacts due to aerosol can cause changes in BUOY, which is susceptible to changes in latent heat release due to changes in condensate (changes in the amount of condensate also impact the r_{cond} term).

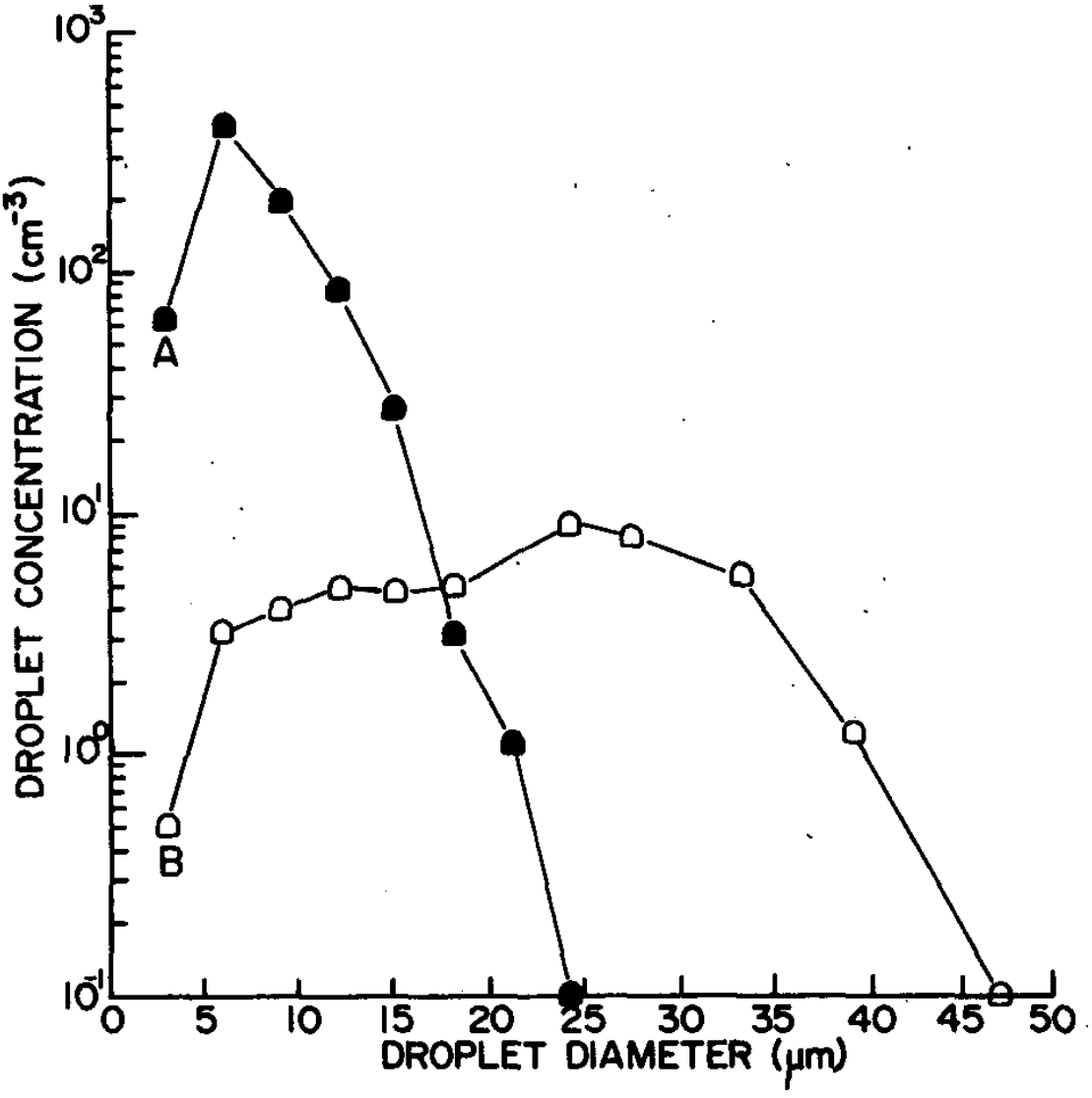

Figure 2.1: Droplet spectra for a continental cumulus congestus cloud (curve A) and similar-sized maritime cumulonimbus cloud (curve B). From Hobbs and Rangno (1985).

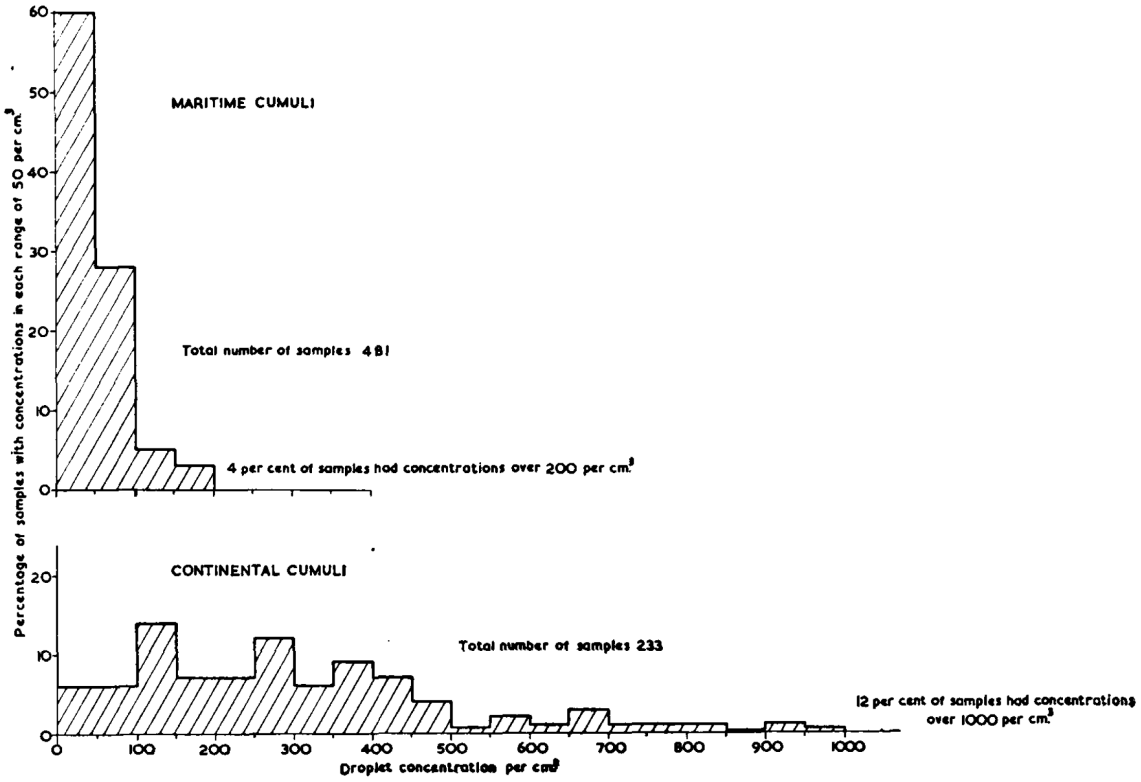

Figure 2.2: Histograms of the percentage of all samples taken in maritime and continental cumuli in which the droplet concentration fell in specified ranges. From Squires (1956).

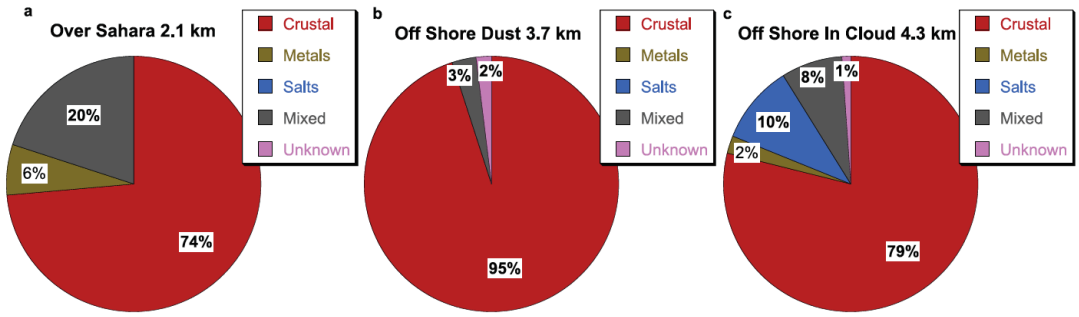

Figure 2.3: Percentage of different particle types by number from 5 Sept 2006 Saharan dust samples during the NAMMA field campaign. Samples include (a) directly over the Sahara, (b) over the Atlantic off the African coast, and (c) composition of residual particles from a cloud embedded in the dust layer. From Twohy et al. (2009).

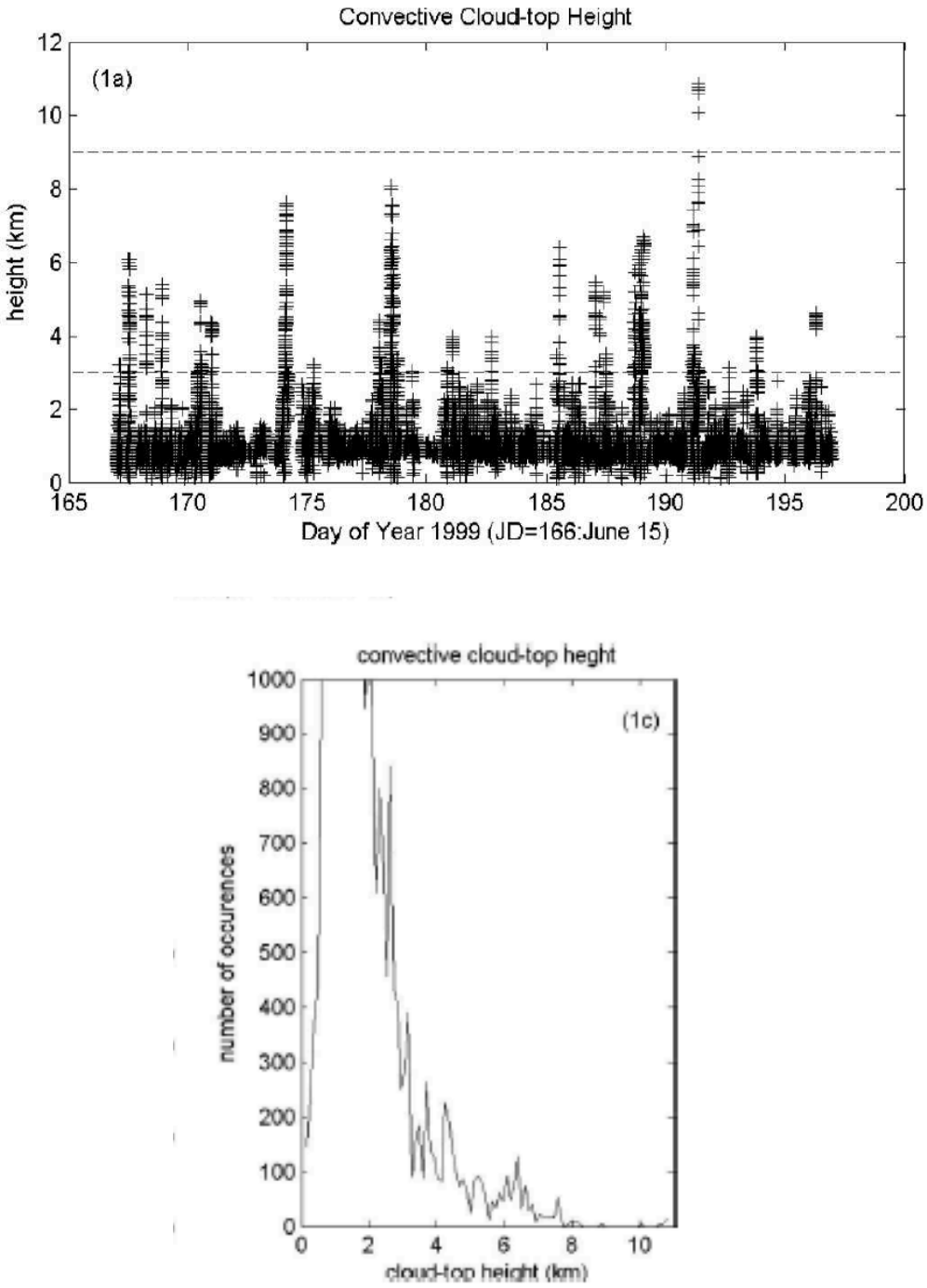

Figure 2.4: Time series (top) and histogram (bottom) of convective cloud-top heights (cloud base below 2 km) from the Atmospheric Research Measurement (ARM) site on Nauru Island in the tropical west pacific. From Jensen and Del Genio (2006).

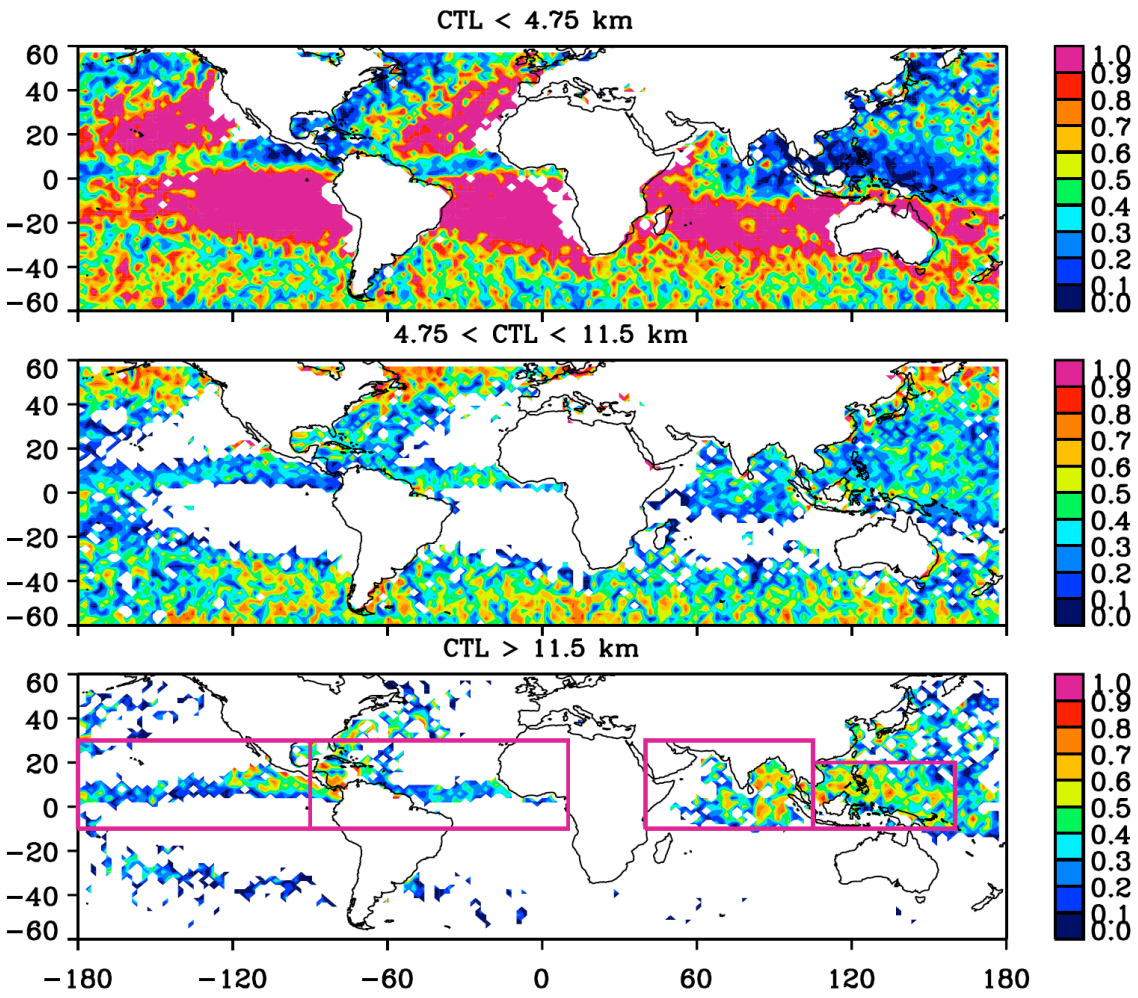

Figure 2.5: Relative frequency of precipitation occurrence of cloud with top heights of less than 4.75 km (top), 4.75 to 11.5 km (middle), and greater than 11.5 km (bottom) from CloudSat. Sum of all three cloud top heights per grid box is unity. From Haynes and Stephens (2007).

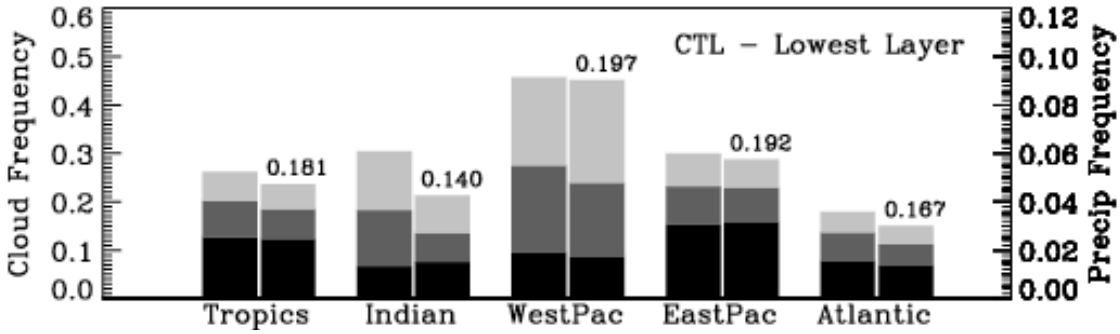

Figure 2.6: Histograms of the frequency of occurrence of cloud top heights for the three modes of tropical convection for 5 regions of tropical oceans. Left column represents frequency of all cloud occurrences and right column represents those precipitating. Darkest color represents low clouds (< 4.75 km), second darkest color represents mid-level clouds (4.75 – 11km), and lightest color represents high clouds (> 11 km). From Haynes and Stephens (2007).

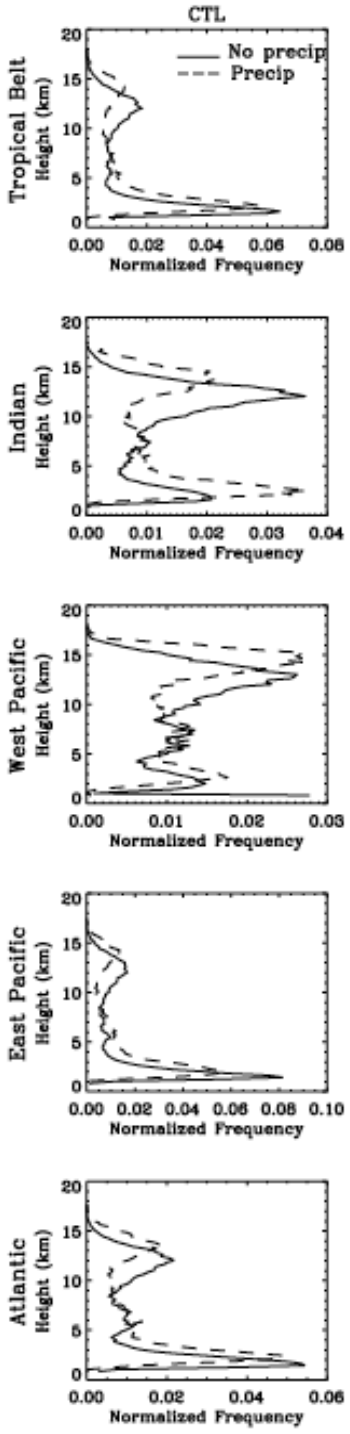

Figure 2.7: Vertical profile of the normalized incidence of the cloud top height in the 5 tropical ocean regions found in figure 2.6. The solid line represents all clouds and the dashed line represents precipitating clouds. From Haynes and Stephens (2007).

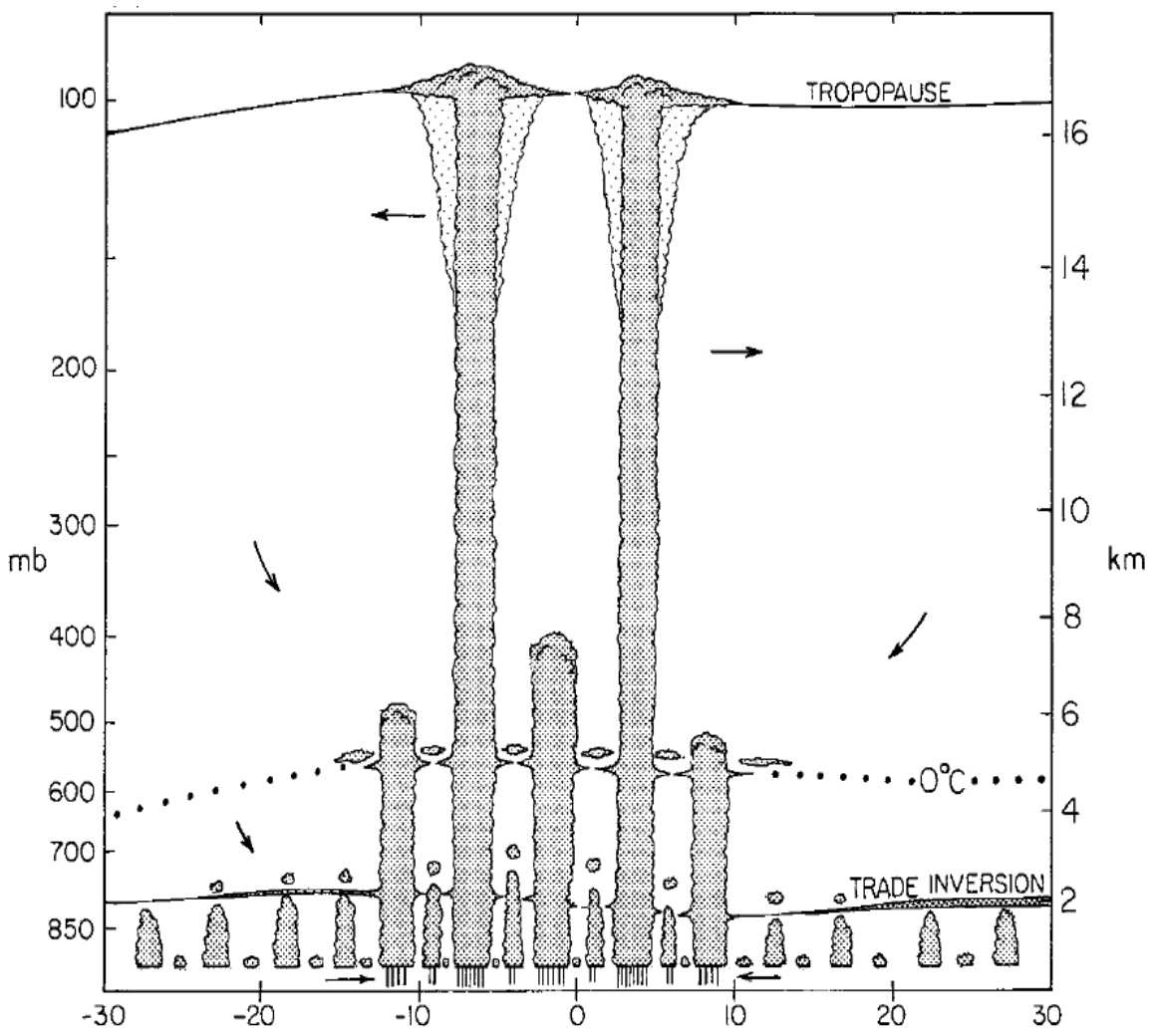

Figure 2.8: Schematic of tropical cloud types and circulation found in the trimodal distribution of convection found in Johnson et al. (1999). Cumulus congestus cloud top in this study are defined to be from 4.5 to 9.5 km in altitude AGL. Three stables layers are indicated, the trade layer, the 0°C layer, and the tropopause.

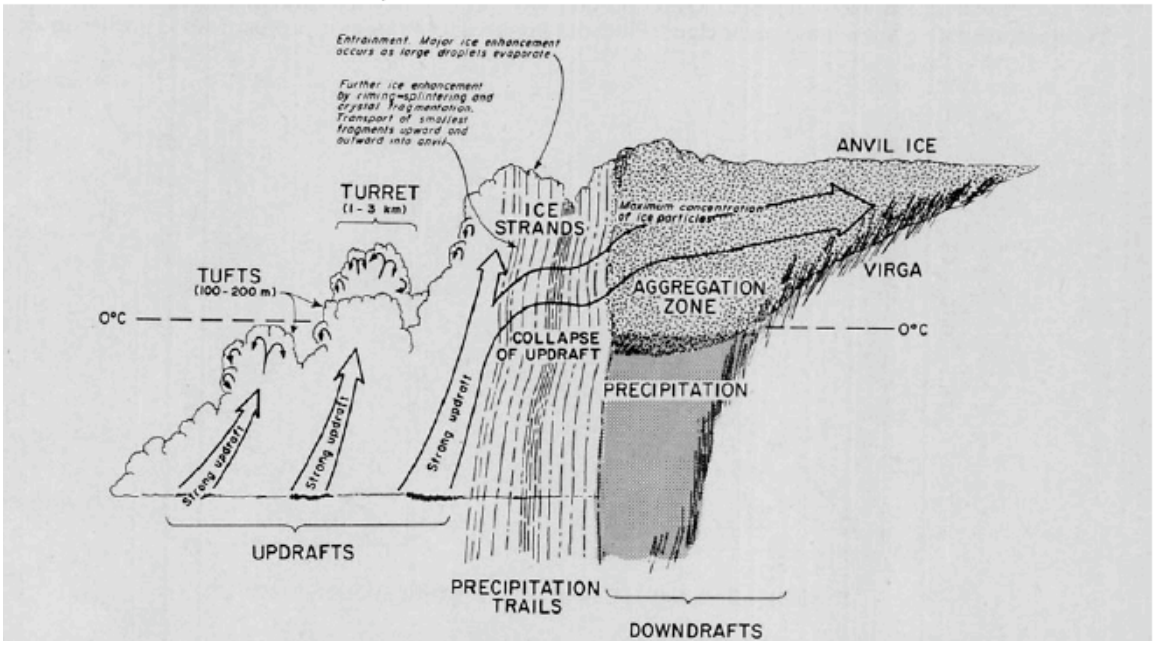

Figure 2.9: Schematic of the conceptual model from Hobbs (1985) for the development of high ice particle concentrations in small cumuliform clouds.

3. METHOD

To achieve the goals of this study of an analysis of AIEs on cumulus congestus clouds, an idealized modeling framework allowing for the development of tropical convection is used. One way to achieve such an examination is through the use of high-resolution CRM simulations in order to capture the microphysical processes active in these congestus clouds and their response to AIEs. The experiment design and model setup, as well as cumulus congestus selection process, are included in this chapter.

3.1 THE RAMS MODEL

The experiment conducted here is similar to that described in van den Heever et al. (2011) (referred to as vdH2011), with differences existing in the domain resolution. The model employed is the Regional Atmospheric and Modeling System (RAMS) (Pielke et al. 1992, Cotton et al. 2003). RAMS is a non-hydrostatic cloud-resolving model with an advanced microphysics scheme (Walko et al. 1995, Meyers et al. 1997, Saleeby and Cotton 2004). It has been used to simulate many different scales of atmospheric phenomena, and their responses to AIEs. This includes tornadogenesis (Lerach et al. 2008), orographic clouds (Saleeby et al. 2009), hail storms (van den Heever et al. 2007), and more.

The advanced RAMS microphysical scheme includes the ability to examine AIEs through a two-moment, bin-emulating bulk scheme. The current RAMS microphysical scheme is described in Meyers et al. (1997) and Saleeby and Cotton

(2004) and will be briefly summarized here because of its importance to the examination of processes in this study.

The two-moment microphysical scheme includes prediction of hydrometeor mixing ratio and number concentration. Processes related to these rely on previously generated look-up tables of conditions obtained using a detailed bin-resolving parcel model. Hydrometeor species include pristine ice, snow, aggregates, graupel, hail, cloud water, and rain water and are represented using a generalized gamma distribution function. The microphysical scheme includes processes important to this study of aerosol impacts on cloud and ice production:

- Heterogeneous cloud droplet nucleation (based the equation below). Ice nucleation due to homogeneous and heterogeneous freezing.
- The ability of all hydrometeors to collect others (except collection by pristine ice), and hence impact the mixing ratio and number concentration, through:
    - Self collection
    - Pristine ice and/or snow collection to form aggregates
    - Ice hydrometeor collection of another ice species and remaining in the same category of ice
    - Liquid collection by ice depending on type and amount of colliding ice and collected liquid species. Mixing ratio, number concentration, and thermal energy produced by the collision process is divided between the input ice category and secondary ice category (graupel if includes cloud, hail if includes rain).
- Collisional breakup, melting, and shedding

- Secondary ice processes based on the Hallett-Mossop process

Saleeby and Cotton (2004) implemented and described recent advancements to the microphysical scheme. The scheme allows the model to predict the cloud droplet number concentration following aerosol activation through the use of look-up tables created from a Lagrangian parcel model run offline (Heymsfield and Sabin 1989, Feingold and Heymsfield 1992). The droplet growth equation is solved iteratively considering the changes in a rising air parcel, including the saturation ratio, temperature, air and droplet solution density, liquid water content, and air pressure. CCN are assumed to consist of ammonium sulfate and are represented by a binned lognormal distribution based on a given number concentration and mean radius. Further details of this parcel model can be found in Saleeby and Cotton (2004).

As mentioned in vdH2011, the number of activated CCN or IN is given by:

$$N_{activated} = N_{available} F_{activation}$$

where $N_{available}$ is the maximum aerosol available to act as CCN or IN based on the $F_{activation}$ factor that is a function of the ambient conditions. The use of this scheme avoids the need to directly prescribe cloud droplet number concentrations in order to investigate AIEs. In this study the concentrations of aerosol available to act as ice nuclei are kept constant.

3.2 MODEL CONFIGURATION

In order to evaluate the CCN effects on tropical convection, vdH2011 and this study used a large domain, two-dimensional CRM model setup that is run to a state of RCE (Tompkins and Craig 1998, Stephens et al. 2003). Over 60% of the energy

removal from the surface of the Earth is by the transport of heat and water vapor by atmospheric motions (convective adjustment), compared to the 40% lost to longwave outgoing radiation (radiative transfer) (Hartmann 1994). This dual-process energy balance common in the Tropics is called radiative-convective equilibrium. Model simulations conducted using the RCE framework are appropriate for idealized tropical experiments due to similarities to the observed thermodynamic and moisture structure of Tropics.

vdH2011 used a two-dimensional grid of 10,000 points at 1 km grid spacing in the zonal direction and 38 vertically stretched points. The differences in this study are in the vertical and horizontal domain size. This model setup includes 65 vertical levels instead of 38, providing greater resolution of vertical convective exchange (especially important to this study). Horizontal resolution remains at 1 km grid spacing but includes only 7,200 points due to computational limitations. Periodic boundary conditions were used along with a rigid top boundary with four Rayleigh absorbing layers to prevent gravity waves from reflecting into the domain and amplifying. A fixed sea surface temperature of 300 K was used. There is no representation of the Coriolis force.

Experiment simulations were initialized with a 0000 UTC 5 December 1992 sounding from the Tropical Ocean and Global Atmosphere Coupled Ocean-Atmosphere Response Experiment (TOGA-COARE). From this the thermodynamic structure of the atmosphere was able to progress and evolve. This included the winds evolving from an initial zero mean wind. Convection was initiated by randomized perturbations to the potential temperature field across the entire

domain below 2 km AGL. Experiment simulations were run for 100 days at a 10-second time step, with RCE achieved after 60 simulation days. Other relevant model options are in table 3.1. The model is allowed to evolve to a RCE environment of tropical clouds over a fixed SST oceanic surface, similar to vdH2011, Stephens et al. (2008), and Posselt et al. (2008). No diurnal cycle was represented as the solar zenith angle was fixed at 50^{o}. The model setup generates moist and dry regions sustained by the circulations between them.

3.3 EXPERIMENT DESIGN

In order to understand the effects of aerosols on tropical convection, this study uses the previously described model setup of simulations of a tropical oceanic environment with the addition of a continuous layer of aerosol that can serve as CCN. This is representative, in an idealized manner, of a Saharan dust event over the Atlantic Ocean or Asian dust event over the tropical Pacific. Aerosols that can serve as CCN only were inserted in the model between 2 - 4 km (observed height of Saharan air layer (SAL), Prospero and Carlson 1981, Sassen et al. 2003, Demott et al. 2003, Cziczo et al. 2004, Prenni et al. 2007) after RCE was achieved and allowed to run for 40 more simulation days. A background aerosol concentration of 25 cc^{-1} was used and a lower minimum limit was placed at 20 cc^{-1}. Layers of aerosol available to act as CCN varied from clean (100 cc^{-1}) to a variety of polluted concentrations (200, 400, 800, 1600 cc^{-1}), similar to previous studies (Xue and Feingold 2006, van den Heever et al. 2006, and vdH2011). This was the only source of aerosol, which was then available to be advected around and removed from the model domain by the

process of activation and precipitation. The aerosol source was then replenished each time step.

From this point forward, the CCN experiments are referred to as CCN-100 (100 cc^{-1}), CCN-200 (200 cc^{-1}), CCN-400 (400 cc^{-1}), CCN-800 (800 cc^{-1}), and CCN-1600 (1600 cc^{-1}) experiments. Apart from the number of particles available to serve as CCN, the experiment setups are otherwise identical.

3.4 CUMULUS CONGESTUS CLOUD SELECTION

As will be seen below, this model setup does produce trimodal convection, including the congestus mode. Cloud was identified where the sum of PSAC (pristine ice, snow, aggregate, and cloud water hydrometeors) was greater than 0.1 g kg^{-1}. This threshold was different than the cloud value of 0.01 g kg^{-1} value chosen by vdH2011 and previous studies (Grabowski et al. 2003). Early work in this study found that increasing the PSAC threshold allowed for a more accurate identification of congestus cloud. From this definition of cloud, cumulus congestus clouds were identified by a continuous column of cloud with specific size and cloud top height requirements, to be discussed below.

A comparison of a sample output of a convective region from the RAMS simulations to a sample from the CloudSat satellite is provided in figure 3.1. This shows that the convective regions captured in these RCE simulations is similar to the observed structure of tropical convective clouds. This includes the depth of convective clouds and presence of convective systems of varying sizes. As found in the RAMS simulations of Posselt et al. (2008) and vdH2011 and observed in Johnson et al. (1996) and Johnson et al. (1999), a trimodal cloud distribution is found to

correlate to three shallow stable layers. This is also seen in the vertical cloud fraction from vdH2011 (figure 3.2): a low cloud mode peak is found at ~2 km (trade wind stable layer), a middle cloud mode at ~ 5 km (0^{o}C level stable layer), and a high cloud mode at ~10 km (the Tropopause stable layer).

Cumulus congestus clouds selected for this study includes those clouds that have cloud bases below (2 km) and cloud tops above the lowest stable layer (4 km) (similar to Jensen and Del Genio 2007). After the initial evaluation of clouds, a maximum cloud top height was placed at 7 km to identify cumulus congestus from deeper convection (cumulonimbus). These thresholds were based on observations in previous studies (Johnson et al. 1999, Jensen and Del Genio 2006, Haynes and Stephens 2007) and correspond well with what is seen in these simulations. These clouds may continue to grow to deep convection or they may not. This study does not distinguish between terminal and transient clouds, but instead focuses on their characteristics and how they change in clean and polluted environments when they are labeled as a congestus cloud.

The freezing altitude in this study was found near 4.6 km, so cumulus congestus cloud tops considered in this study could be above or below the freezing level. The freezing level in these simulations is similar to recent preliminary findings from the Ice in Cumulus – Tropics (ICE-T) field campaign (personal experience). Figure 3.1 shows several examples of cumulus congestus clouds in a convective zone of the model simulations. The freezing level can be seen in a plot of domain-average static stability (figure 3.3), where in the subsiding regions a clear trade and freezing level stable layer are seen. In the broad ascending regions, the

stable layer is found slightly higher up compared to the subsiding region. A cloud top upper limit was placed at 7 km because of the low number of congestus cloud occurrences in the 7 to 9 km cloud top height range.

Cumulus congestus clouds were found by determining the cirrus, upper, and mid level clouds from the cumulus below them. Searching from the top of the atmosphere to the surface, this was completed by removing those clouds that do not meet the cloud depth restrictions described above. Clouds properties were then obtained from the cloudy columns identified using this method. Ten simulation days at 5-minute interval output were analyzed in this large cumulus congestus cloud sample.

Table 3.1: Model setup for the RAMS cloud resolving model simulations.

	Model Setup
Grid	Arakawa C grid (Mesinger and Arakawa 1976) 2D Simulations Horizontal: Δx = 1 km 7,200 grid points Vertical: 65 vertical levels: Δz variable Model Top: ~ 26 km 11 levels below 1 km AGL
Initialization	0000 UTC 5 Dec 1992 TOGA COARE sounding with zero mean wind Randomized perturbations to the potential temperature field
Time Step	10 s
Simulation Duration	100 days; aerosol layer introduced at simulation day 60
Microphysics Scheme	Two-moment bulk microphysics (Meyers et al. 1997) Aerosol scheme (Saleeby and Cotton 2004)
Convective Initiation	No cumulus parameterization: convection resolved
Boundary Conditions	1) Periodic boundary conditions 2) Fixed lower oceanic boundary (SST = 300 K) 3) Fixed upper boundary with Rayliegh absorbing layers
Turbulence Scheme	Smagorinsky (1963) deformation-K closure scheme with stability modifications by Lilly (1962) and Hill (1974)
Radiation Scheme	Harrington (1997) scheme updated every 5 minutes
Surface Scheme	LEAF-2 (Walko et al. 2000)

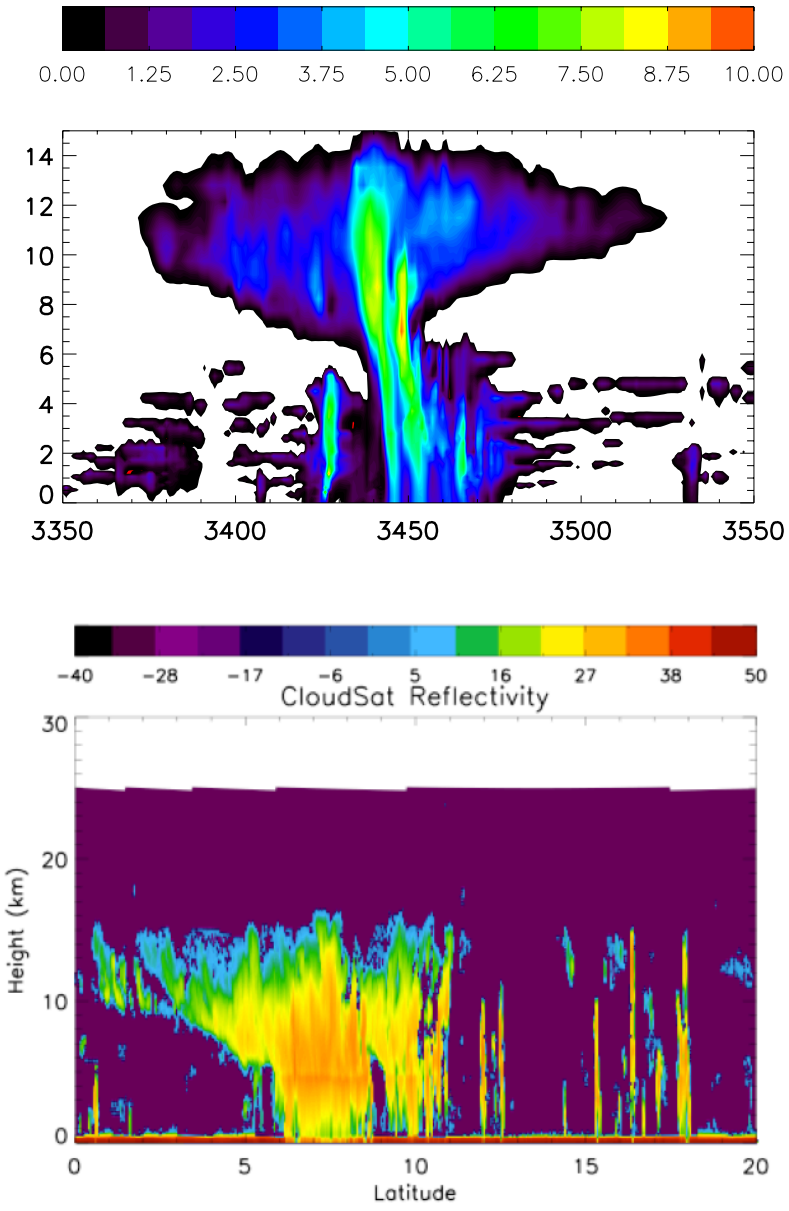

Figure 3.1: Figure provided for a comparison of a field of deep convection produced by the RAMS model simulations (top) used in this experiment to CloudSat observations (bottom) (CloudSat observations courtesy of Rachel Storer).

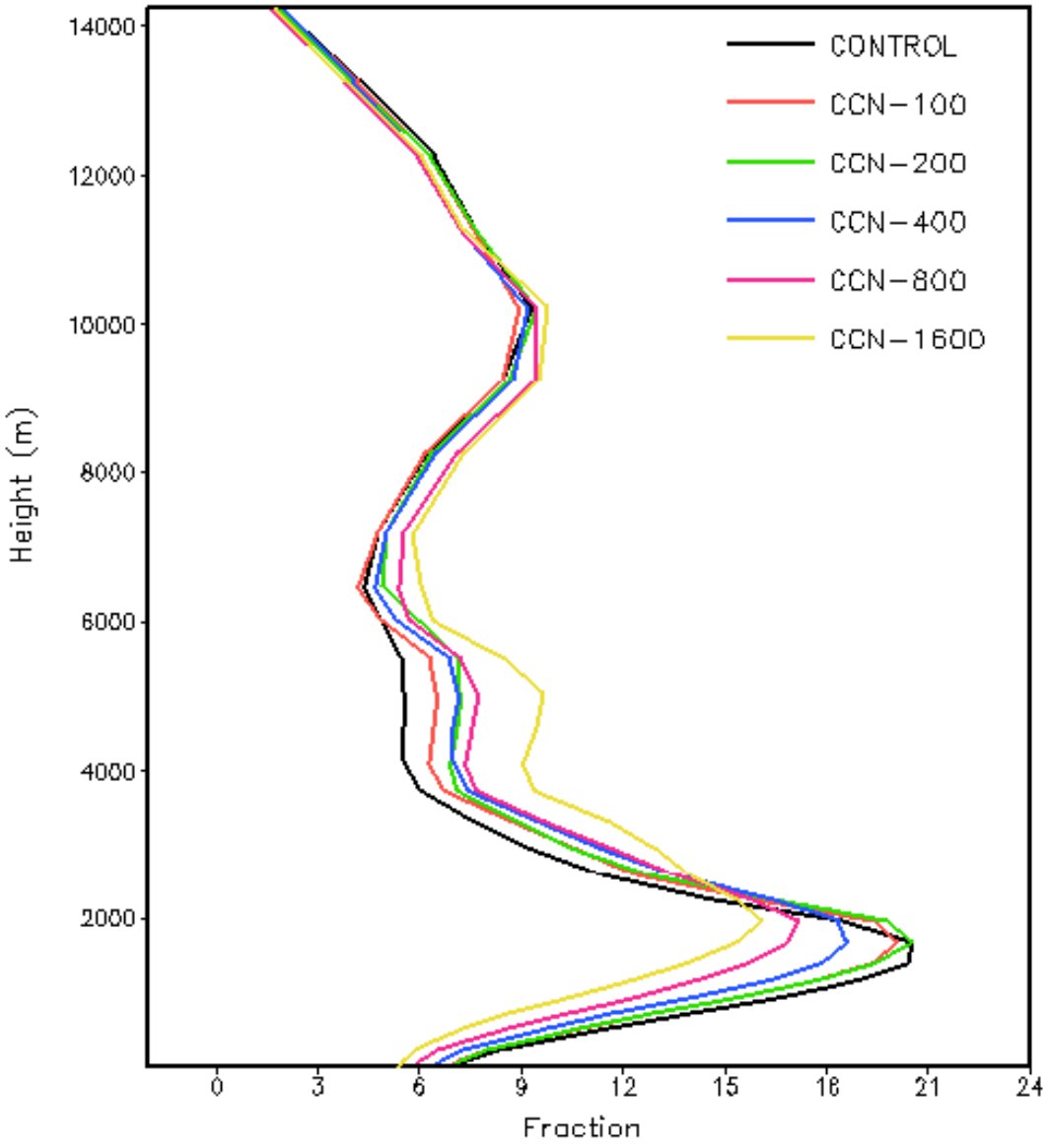

Figure 3.2: Cloud fraction (total condensate > 0.01 g/kg) for varying CCN concentration simulations in a large RCE RAMS model simulation. From vdH2011.

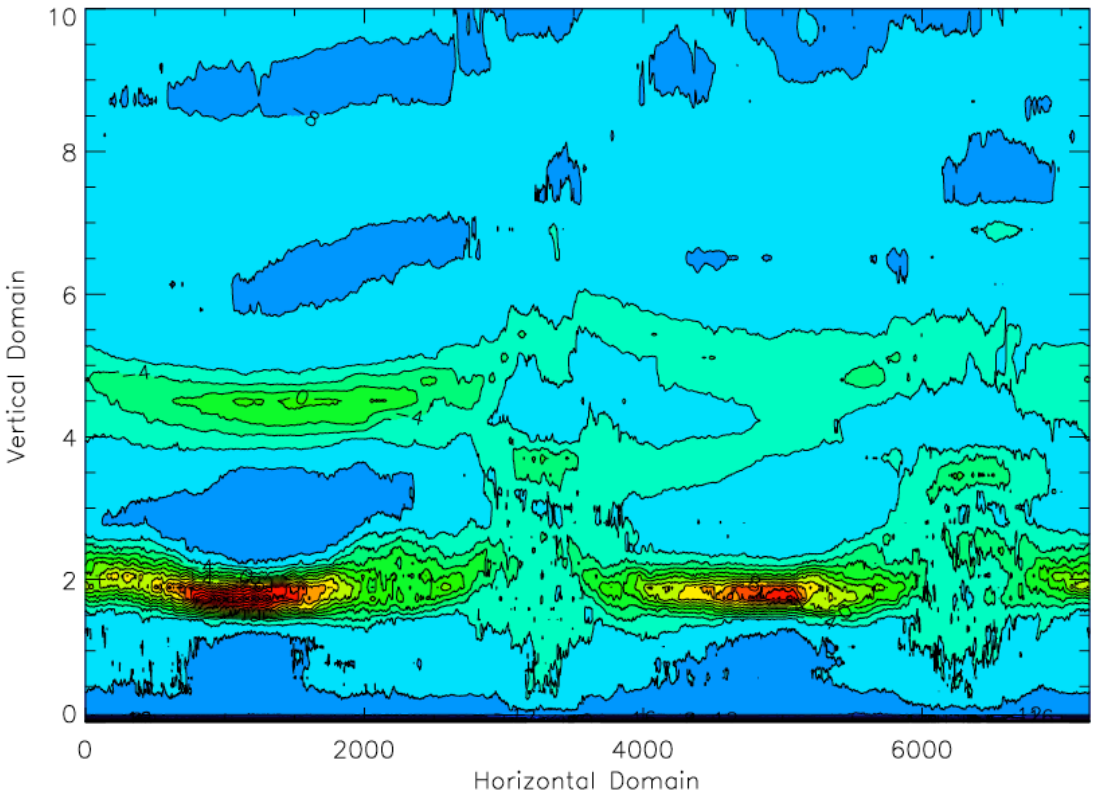

Figure 3.3: Contour plot of dT dZ^{-1} (K m^{-1}) across the 7200 km horizontal domain and 10 km vertical domain. Red indicates the greatest stability.

4. RESULTS

4.1 A SINGLE CUMULUS CONGESTUS CLOUD

The model setup in this study allows for the development of two broadly rising regions, in which the trimodal distribution of clouds is evident. A comparison of a sample output from one convective region from these experiments with observations supplied from CloudSat provides justification that the model is able to reproduce the trimodal distribution of convection appropriately (figure 3.1). Cumulus congestus cloud base is generally found to be near 1 km AGL. The cumulus congestus clouds occurring in the model had an average updraft speed of at most several m s^{-1}, as will be shown in figure 4.4 in section 4.3. Observations have found similar updraft speeds in sampled cumulus congestus (Heymsfield et al. 1979), though in-situ observations of congestus are very few.

An example of one of the congestus clouds simulated by the model is shown in figure 4.1. The cloud initially remains below the freezing level (approximately 10 to 15 minutes into its lifetime, top panel of figure 4.1), but then rapidly grows to near 6 km (approximately 20 minutes, middle panel of figure 4.1) before becoming slightly higher than the congestus definition used in this study (approximately 7.5 km) at 25 minutes (bottom panel of figure 4.1) and becoming deep convection at 30 minutes.

This cumulus congestus sample is transient because it became deep convection after the cumulus congestus stage. The following chapters will provide

insight into the variations in cumulus congestus cloud characteristics with varying aerosol and the resultant growth about the freezing level.

4.2 CLOUD TOP DISTRIBUTION

Section 4.1 presented an example of a cumulus congestus cloud captured within this modeling study. We now examine the entire population of congestus clouds developing in these simulations. Understanding the overall congestus population characteristics is useful in assessing the effects of CCN concentrations on these clouds. Figure 4.2 is the temporal average of the percentage of the domain containing cumulus congestus clouds, plotted by altitude of the cloud top. The congestus were plotted by cloud top in this figure in order to evaluate frequency of cloud and the maximum heights of them. The dashed line corresponds to the freezing level of 4.6 km in these model simulations. All CCN experiments show two peaks in cloud top, one above and one below the freezing level. The lower peak (4 km in altitude, the lower cloud top threshold) corresponds to those cumulus congestus clouds that have warm microphysical processes only and have grown past the lower, trade wind stable layer at approximately 2 km (figure 3.3). However, at the point in time that they are included in this sample, they are not yet buoyant enough to extend beyond the freezing level. With increasing CCN concentration, it is evident that there is increasingly more cumulus congestus cloud tops in the domain, with the exception of the CCN-800 experiment.

Above the freezing level, generally, cumulus congestus clouds cover more of the domain. This increase in coverage results in a higher mean cloud top frequency in the more polluted scenarios (again with the exception of the CCN-800 scenario).

Congestus are only examined here when their cloud tops fall within the vertical altitude constraints mentioned chapter 3. This means that though there are dual peaks in cloud tops in figure 4.2 due to stationary cloud above and below the freezing level, some of these clouds may develop into deeper convection in their lifetime.

The variation in the frequency of cloud top with CCN concentration suggests that variations in aerosol concentrations result in some microphysical and dynamical changes to cloud. The increase in mean cloud top frequency occurs in all CCN experiments except CCN-800, which has fewer cloud tops than CCN-100. This result in this experiment is being investigated further outside of these results. Cumulus congestus cloud top frequency is cumulatively shown in figure 4.3, which is a bar graph of the vertically integrated cumulus congestus cloud top counts for each CCN concentration experiment shown in figure 4.2. As the CCN concentration increases, the total congestus cloud frequency generally increases. Similar trends were found when the statistics were separated for cloud tops above and below the freezing level (not shown).

Above the freezing level the cloud top peak frequency varies in altitude with increasing CCN concentration but generally increases. CCN-100 has a cloud top peak near 4.8 km while CCN-200 has a peak near 5.5 km. As the CCN concentration increases to 400 and 800 cc^{-1}, the peak lowers below the CCN-200 peak, but remains above CCN-100's peak and is vertically broader. The peak continues to increase in altitude from the CCN-400 through to CCN-1600 experiments and continues to broaden. The vertical broadening of the upper level peak shows that more clouds

are peaking in multiple altitudes, instead of the more narrow range of the CCN-100 and CCN-200 experiments. The CCN-1600 cloud top distribution nearly loses the dual peak (one above and below the freezing level) shape as its upper peak broadens and increases in altitude.

More numerous, higher cloud tops are generally found with increasing CCN concentration. More numerous, deeper clouds indicate that some process is allowing these congestus clouds to reach higher levels throughout the 4 to 7 km cloud top region. The increasing range of the cloud top heights with increasing CCN concentration may indicate a complex relationship of varying processes that are influencing cloud top above the freezing level. These two points would suggest that increasing the CCN concentration somehow affects the thermodynamical and dynamical response in these clouds. The following sections investigate these processes, including the formation and modification of cloud and ice hydrometeors.

4.3 UPDRAFTS

The time- and domain-averaged updraft speeds of congestus as a function of height and of increasing CCN concentration are found in figure 4.4. Figure 4.4a shows the vertical profile of the average updraft speed per CCN experiment while figure 4.4b shows those greater than 1 m s^{-1}. This figure demonstrates that there is an increase in the updraft speeds below 5 km with increasing CCN concentration. The clearest increase occurs from the 100 to the 400 experiments, followed by a slight increase in the CCN-800 to the 1600 experiments. This appears in both threshold values of the updraft speeds, although more clearly in the stronger updraft case. There are two maximum peaks in updraft speeds. The lower peak

generally follows the trend of the increase in cloud top frequency shown in figure 4.2. This indicates that an increase in updraft speeds in the more polluted cases is resulting in more numerous cloud tops below the freezing level.

Above 5 km, trends in the updraft speed as a function of CCN become more complex. At approximately 5.5 km, the updraft speed begins to decrease in the most polluted case, followed by a consistent decrease in maximum updraft speed peak height from polluted to clean. This at first glance may seem to contradict the results of more numerous cloud tops above the freezing level for the more polluted cases evident in figure 4.2. However as we will see later, increases in the total condensate amounts with increasing aerosol concentration, while positively enhancing cloud top frequencies, will act to reduce updraft strengths. Further evaluation as to why there is an increase in updraft speeds below the freezing level and a decrease above this level will follow in the next sections.

4.4 CHARACTERISTICS OF CUMULUS CONGESTUS CLOUDS

Provided in this section is an analysis of the domain- and time-averaged distribution of cloud hydrometeors and the microphysical processes which impact them. Analysis of the changes in cloud water and ice due to aerosol effects is necessary in order to understand the updraft speed and cloud top response mentioned previously. Changes due to latent heating associated with the production of the cloud condensate, as well as drag effects of condensate, will influence the BUOY term. Figures 4.5 through 4.8 show the vertical distributions of domain- and time-averaged mixing ratio (g kg^{-1}), number concentration (m^{-3}), and average hydrometer diameter (mm) of cloud water, rain water, pristine ice, snow,

aggregates, graupel, and hail in cumulus congestus cloud for the CCN experiments. Figures 4.9 through 4.14 include vertical distributions of domain- and time-averaged microphysical processes involving these species, including nucleation of cloud droplets, vapor diffusion onto cloud droplets, nucleation of ice, vapor diffusion onto ice, riming of cloud water, riming of rain water, and melting of ice species, respectively. Many of the following figures included in this study are similar to these plots in that they are vertical profiles of the domain- and time-averaged variable of interest. When this is not the case, the figure will be described.

4.4.1 CLOUD AND RAIN WATER

According to previous studies of AIEs in cumulus clouds, increasing the CCN concentrations will impact the amount and vertical distribution of cloud water and other hydrometeor species (Twomey 1974 and 1977, Albrecht 1989, vdH2011, Seifert and Beheng 2006, Khain 2005, etc). Here, cloud water mixing ratio shows an increase with increasing CCN concentrations (figure 4.5a). This mixing ratio increase results from a delay of rain formation processes (second AIE) caused by a reduction in the rates of collision and coalescence processes that allows for more cloud water mass to remain in the cloud. This delay is further confirmed by the increase in cloud droplet number concentration (figure 4.5b) and a decrease in the mean size of cloud droplets (figure 4.5c), all characteristics of typical aerosol indirect forcing. This is also confirmed is a decrease in rain mixing ratio (figure 4.5d).

The vertical profile of cloud mixing ratio has maximum values near 3.5 to 4 km and 5.5 to 6 km. These maxima correspond to the dual peaks in cloud top

frequency found in figure 4.2, indicating that cloud water is amassed at these altitudes due to lofting and subsequent detrainment. As previously mentioned, this study found more numerous, smaller cloud droplets and a larger cloud mixing ratio in the more polluted scenarios. The cloud droplet number concentration is ten times larger in the CCN-1600 experiment than the CCN-100 experiment, and the mean cloud droplet diameter is twice as large in the CCN-100 experiment compared to the CCN-1600 experiment. There is nearly 50% more cloud mixing ratio between the most clean and polluted scenarios.

Rain mixing ratio shows a decrease with increasing CCN concentration (figure 4.5d) in keeping with aerosol indirect theory (Albrecht 1989). The least amount of rain mixing ratio occurs above the freezing level. The maximum amount of rain mixing ratio occurs near 2 km, the congestus cloud base minimum requirement. Rain is formed through the collision and coalescence of cloud droplets, the collection of cloud water by raindrops, the melting of ice hydrometeors, and the shedding of melt water. Removal processes, such as riming by ice hydrometeors and evaporation, also affects the total rain water mass. A reduction in rain with increasing CCN concentration would result from an increase or decrease in one of these processes. These relationships are examined below.

Also included in figure 4.5 is rain droplet number concentration (figure 4.5e) and rain droplet mean diameter (figure 4.5f). Rain mixing ratio decreases with increasing CCN concentration. This decrease is not as great as the increase in cloud mixing ratio in the more polluted cases, being at most 25%. Rain mass is most likely greatest in the lower altitudes because of the contributions from the melting of ice

and a reduction in the riming of rain. Raindrop number concentration also decreases with increasing CCN concentration and is greatest near 3.5 km in altitude, decreasing above and below this point. A change in the vertical gradient of rain mixing ratio occurs at approximately 4 km. As will be discussed in section 4.5, this is due to collection by hail above the melting level. Raindrop number concentration decreases toward the surface while the mean diameter increases. Similar results have been observed in other studies, including Storer et al. (2010) and Berg et al. (2008). This decrease toward the surface is a result of the evaporation of the smaller raindrops first, which shifts the raindrop distribution to greater mean diameters. This would suggest that with increasing CCN number concentrations, decreases in rain mixing ratio and number concentration result, however the rain droplets are larger due to their collection of more readily available cloud water, as well as the preferential evaporation of the smallest raindrops.

Overall an increase in the amount of cloud water has occurred in the more polluted experiments. This increase results in more cloud water throughout the cumulus congestus clouds, as is seen in figure 4.5a, and has implications for ice formation aloft. As we have seen, there is an increase in the updraft speeds in these more polluted cases below the freezing level.

Increased updraft speeds along with the increased cloud water mixing ratio results in more cloud water mass being lofted above the freezing level. This lofted, increased supercooled cloud water mass is available to become ice, either through nucleation or riming. Several studies have hypothesized that this greater supercooled cloud water mass may lead to greater convective invigoration upon

freezing (Khain 2005, van den Heever et al. 2006). However, the greater amounts of cloud water in the more polluted cloud cases also enhance the condensate drag, in competition with this latent heat based invigoration. These competitive processes will be investigated further in section 4.5 and 4.6.

4.4.2 PRISTINE ICE, SNOW, AND AGGREGATES

Changes in cloud water mixing ratio through the second AIE have impacts on the ice hydrometeors as their formation frequently involves cloud water. The time- and domain-averaged vertical profiles of pristine ice, snow, and aggregates are shown in figure 4.6. This plot demonstrates that the majority of PSA mixing ratio is due to snow (~ 30%, figure 4.6d) and aggregates (~ 70%, figure 4.6g), though this peak mixing ratio value is an order of magnitude less than that for cloud water or rain water in these regions of the cloud. As the CCN concentration in each experiment increases, so does the average value of PSA mixing ratio due to an increase in the snow and aggregate mixing ratios. Pristine ice shows little trend in its mixing ratio with increased CCN concentration.

Also important are the number concentrations and diameters of ice hydrometeors as these characteristics impact the amount of growth of each hydrometeor species through vapor diffusion and riming, as well as influencing their ability to melt. As snow and aggregate mixing ratios increase, the mean diameter of these hydrometeors decreases (figures 4.6f, i, respectively) while the mean diameter of pristine ice increases (figure 4.6c). An increase in snow and aggregate number concentrations also occurs with increased CCN (figures 4.6e, h, respectively).

4.4.3 GRAUPEL AND HAIL

Graupel mixing ratio shows an increase in mean value and a lowering of the peak mixing ratio value with increasing CCN concentrations (figure 4.7a). Graupel growth is due to the collection of cloud droplets by graupel. Increased cloud water mixing ratio means that more cloud water is available for collection. The hail mixing ratio generally shows a decrease with increasing CCN concentration (figure 4.7d). Hail forms from freezing of raindrops, the collection of rain on ice hydrometeors, and the melting of graupel. Here it would be expected that a decrease in rain mixing ratio would result in a decrease in hail mixing ratio. PSA (dominated by aggregates) and hail have the largest time- and domain-averaged mixing ratio of the ice hydrometeors, with graupel being an order of magnitude less.

Graupel and hail are generated by collection of cloud and rain, respectively. Hail also can result from the melting of graupel. Graupel number concentration (figure 4.7b) and diameter (figure 4.7c) show changes with CCN concentration according to altitude in the cloud. Overall, graupel is a very small mass in these clouds compared to snow, aggregates, and hail. Hail number concentration (figure 4.7e) and diameter (figure 4.7f) show that with increasing CCN concentration the particles are smaller and less numerous. Figure 4.7d indicated that CCN-200 experiment did not follow the trend of the other CCN experiments. This appears to be due to having diameters near the CCN-100 experiment, but concentrations near the CCN-400 experiment, resulting in less hail mixing ratio than expected. In section 4.5 it will be shown that this is due to the collection of rain.

The separation of the analysis of cloud and ice particles is important in terms of their formation and modification. Each individual hydrometeor process has different impacts on the thermodynamic and subsequent dynamic structure of these clouds. These impacts on cloud ice and water in more polluted scenarios suggest that microphysical changes will impact the dynamics of the cloud as was seen in the updraft speed and cloud tops in section 4.2 and 4.3. The processes that contribute to these microphysical and thus thermodynamical changes will be discussed in the next section.

4.5 MICROPHYSICAL PROCESSES

Section 4.4 discussed the distribution of cloud and ice hydrometeors in these cumulus congestus clouds. This resulted in the changes to the cloud hydrometeor species in the more polluted scenarios as found in table 4.1.

The time- and domain-averaged vertical profiles of total liquid and total ice condensate mixing ratio both show an increase in condensate aloft in the more polluted cases (figure 4.8a and b, respectively). In the lowest levels of the total liquid condensate mixing ratio, this trend does not appear due to the contribution of the rain mixing ratio, which is decreasing opposite to cloud water. The increased ice mass aloft occurs as the result of increased cloud water, as discussed previously.

The spatially- and temporally-averaged total condensate values are dominated by the liquid water contributions, as can be seen in comparing figure 4.8a and c. The average liquid water mixing ratio is an order of magnitude larger than the average ice condensate mixing ratio, indicating that there is relatively less

ice than cloud water and rain, even above the freezing level in these cumulus congestus clouds.

Processes that contribute to the formation of cloud water include the nucleation of and vapor diffusion onto those cloud droplets. As previously discussed, the average cloud water mixing ratio profile showed increasing cloud water mass with increasing CCN concentration. As the number concentration of smaller cloud droplets increases with increasing CCN concentrations, a delay in the warm rain process results in retention of cloud water mass. Figure 4.9a shows a decrease in the nucleation of cloud water, but an increase in the rate of vapor diffusion (figure 4.9b) onto cloud droplets in the polluted environment. Initially an increase in the rate of nucleation of cloud droplets would need to occur to create more, smaller droplets. However, once cloud formation has begun, competition for the available water vapor occurs between the nucleation of cloud droplets and the vapor diffusion onto the existing drops. This competition results in an increase in the vapor diffusion onto cloud droplets at the expense of the nucleation of new cloud droplets with increasing CCN. This occurs as a result of the increased surface area associated with the more numerous cloud droplets in the more polluted cases.

Below and above the freezing level, the time- and domain-averaged nucleation of cloud water shows a decreasing trend with increasing CCN concentration. Vapor diffusion onto cloud droplets is seen to increase with increasing CCN concentration, though the cases of CCN-800 and 1600 differ little. This limited increase in vapor diffusion in the more polluted cases results in the total of both the nucleation of cloud droplets and vapor diffusion onto cloud

droplets to not increase near the peak vapor diffusion value (figure 4.9c). It does increase in value from the CCN-100 to 400 experiments, but because similar values of vapor diffusion in the more polluted cases, a decrease in nucleation in the more polluted cases results in a decrease in their combined total. As will be seen later in the discussion of latent heat release from these processes, the convergent trend is also evident. This trend was also apparent in the updrafts previously shown (figure 4.4). It is also important to note that the overall rate of both processes are much greater than those for ice, as will be discussed next.

Once cloud water is formed, the development of rain may occur as well as the formation of ice hydrometeors. The average rain mixing ratio was found to decrease as a result of the decreased size of cloud droplets and the subsequent reduction in the efficiency of the collision and coalescence processes. The average rain droplet size and number concentration is also affected by the presence of ice due to collection by ice, and thus will be discussed following an introduction to the processes that affect ice production.

As previously discussed, an increasing amount of PSA (cloud ice) and graupel mass occurred in the more polluted conditions, which is opposite to the trend in the hail mass. However, this results in more ice mass in the more polluted scenarios (figure 4.8b). In these cumulus congestus clouds, ice is initially heterogeneously nucleated as pristine ice due to the temperatures at cloud top. Figure 4.10 is a vertical profile of the nucleation of pristine ice. It shows a very small nucleation rate and a mixed trend with increasing CCN concentration. This is very similar to the nucleation of cloud water, where ice nucleation occurs but then competes with

vapor diffusion for the available water vapor after the initial stages of development. Ice nucleation also peaks near the cloud top of these cumulus congestus clouds.

Investigation into one pathway for hydrometeors evolving after ice nucleation involves an examination of vapor diffusion. Figure 4.11 provides the time- and domain-averaged vertical profile of vapor diffusion rates onto all ice hydrometeors. Figure 4.11a is the average vapor diffusion onto all ice hydrometeors. It contains two peaks, one near 4 km and one near 6 km. The peak above the freezing level is due to vapor diffusion onto pristine ice, snow, and aggregates and increases with increasing CCN concentration. In comparing the individual hydrometeor diffusion rates it is evident that this is due primarily to diffusion onto snow. All three species however show an increase in the rate of vapor diffusion with increasing CCN concentration. This is similar to the scenario of cloud droplets, where more numerous, smaller hydrometeors result in greater surface area available on which to diffuse vapor.

The lower peak is due to the vapor diffusion onto graupel and hail. Graupel shows an increase with increasing CCN concentration, which is opposite to that of hail that shows a slight decrease with increasing CCN concentration. This peak is below the freezing level and occurs where these large ice particles jointly melt and collect vapor. This is shown to compete with cloud water vapor diffusion in figure 4.9b, where a slight decrease in vapor diffusion onto cloud water occurs. Vapor will preferentially diffuse to the ice hydrometeors due to the lower saturation vapor pressure over ice.

These variations in the rate of vapor diffusion with CCN concentration are the result of the changes in the size distribution of each hydrometeor. The increase in number concentrations of snow and aggregate particles, even though smaller in size, creates more total surface area onto which to diffuse vapor. A similar situation exists with graupel. A decrease in the rate of vapor diffusion onto hail occurred due to less surface area available because of fewer particles, even though they were larger. It is important to note that the overall rate of vapor diffusion onto ice is much less than that onto cloud water.

Once cloud water and ice begin to form and interact, processes involving the amalgamation of hydrometeor species become more important. These processes include riming of cloud water, riming of rain water, and the melting of ice. The riming of cloud water is presented in figure 4.12. Once an ice hydrometeor rimes cloud water, the cloud water often freezes thereby releasing latent heat. As we have seen, hail has the largest size, number concentration, and mixing ratio of all the ice species. Hail mixing ratio decreased in the more polluted cases. Figure 4.12a shows the total rate of riming of cloud water, which is dominated by the rate of riming by hail (Figure 4.12e). There appears to be no significant trend with increased CCN concentrations. The other ice species (snow, aggregates, and graupel) are an order of magnitude less in the riming rate but show an increase in riming with increased CCN concentration. In the polluted scenarios, there is more cloud water available to be collected. This is reflected in the snow, aggregate, and graupel riming rate of cloud water. However, this is not the case in the dominant cloud water riming species of hail.

The riming rate of rain leads to changes in the mass of water on ice hydrometeors, similar to riming rate of cloud water. Figure 4.13 is the time- and domain-averaged vertical profiles of the collection of rain by ice hydrometeors. The rate of the riming of rain on hail decreases with enhanced CCN concentrations because less rain is available to be collected in the polluted cases. This figure thus shows a similar trend with changing CCN concentration as the hail mass in figure 4.6 showed. The rate of collection of rain water by hail is the largest average ice species rate but riming by snow and the other ice species also contribute. Snow, aggregates, and graupel hydrometeors rime more rain with increasing CCN concentration. This appears to be a function of the increased mass of those species already in existence and their ability to collect rain.

Another process important in influencing liquid water and ice is melting (figure 4.14). Melting is a function of the amount of surface area of an ice species. Most of the melting here is found associated with hail, though graupel and aggregates also contribute to melting. Hail shows little trend in melting with increased CCN concentration, similar to the mixing ratio trends seen previously. However, aggregates, graupel, and snow increase in mixing ratio in the polluted conditions in this study, and thus have increased contributions to melting due to the increased available ice content.

4.6 CONVECTIVE INVIGORATION

In the previous sections, the changes in the cloud hydrometeor species and the processes that affect them through variations in aerosol concentrations were investigated. These changes are microphysical, and result in a thermodynamic and

dynamic response in the cumulus congestus clouds examined here. Changes in the updraft speed and cloud top heights occurred and appear to be linked to these microphysical changes. We now investigate the response of cloud dynamics to these changes in cloud hydrometeor species.

Examination of the overall cloud response to aerosol induced microphysical changes includes the evaluation of the BUOY term in the w-momentum equation (equation 5). The buoyancy term includes θ_v differences in the cloudy air parcel from the background state. This difference can be affected by an increase in θ_v associated with a phase change in the cloudy air parcel. The condensate negative contribution is due to the drag arising from the total amount of condensate occurring within the updraft and effects buoyancy negatively.

4.6.1 LATENT HEAT RELEASE - VAPOR

This section discusses the latent heat release and subsequent convective invigoration occurring in these cumulus congestus clouds due to nucleation of and vapor diffusion onto cloud water and ice particles. Cloud water formed in the lower portions of the congestus will be lofted and be available to impact the upper portion of the cloud during growth. If cloud water is lofted above the freezing level, it becomes available to nucleate ice and be collected by riming by ice species. If a process below the freezing level changes due to the aerosol environment, this can have impacts on the upper levels of the cloud.

Figure 4.15 is a vertical profile of the average latent heat release due to the nucleation of cloud droplets and ice crystals and vapor diffusion onto cloud droplets and ice crystals (referred to as LHR-VAP). The release of energy by nucleation of

cloud droplets as well as the vapor diffusion onto cloud droplets was found to be much greater than that associated with the ice species. This is important in terms of the latent heat release because the cloud water processes thus dominate the overall response in LHR-VAP.

Below the freezing level, LHR-VAP generally shows an increase with increasing CCN concentration. A large increase is seen with increasing CCN concentrations from 100 through to 400. However, once a CCN concentration of 800 and 1600 was used, an increase in LHR-VAP was not seen. This trend was also evident in the total of the nucleation of and vapor diffusion onto cloud droplets.

The processes of nucleation and vapor diffusion compete for available water vapor. Each process releases latent heat, which together dominates the LHR-VAP response compared with those associated with ice. Cloud water processes below the freezing level thus control LHR-VAP. When these two processes were examined in section 4.5 (figure 4.9), a decreasing trend with increasing CCN was found in nucleation rates while an increasing trend was found in vapor diffusion onto cloud droplets. However, for the CCN-1600 experiment, the increase in vapor diffusion was not as great as in the less polluted cases. This was due to a small increase in the surface area available for vapor diffusion in the more polluted cases because of the increasingly smaller cloud droplets occurring in the more polluted case, even though number concentrations were enhanced. This trend is reflected in figure 4.9c and similarly in the LHR-VAP response in the most polluted cases in figure 4.15. This is also why there is not as great of a change in updraft speed in the lower cloud levels for the more polluted cases. A limited source of LHR-VAP due to vapor

diffusion onto cloud water in the most polluted cases resulted in convergent trends in updraft speed.

Latent heat release due to vapor diffusion onto cloud droplets and ice crystals and nucleation of cloud droplets and ice hydrometeors also occurs near and above the freezing level, but rapidly decreases with increases in altitude. As previously discussed, a general increase in latent heat release in the more polluted scenarios occurred. This is shown best near the peak in LHR-VAP located near 3.5 km in altitude. Near the freezing level, this trend is more complex. While CCN-100 has the lowest value, the higher CCN concentration LHR-VAP results are mixed. And above this level up to cloud top at 7 km, this trend becomes indistinguishable.

One would think that this variation in trend would result in fewer clouds at higher levels because of the lack of upper level invigoration. However, convective invigoration in the lower levels enhances transport of cloud water into the upper level of the cloud. Though a strong LHR-VAP trend in polluted cloud does not occur near and above the freezing level, there is still an increase in the frequency of cloud tops as seen in figure 4.2 and an increase in cloud water, as seen in figure 4.5. Hence the more frequent cloud existing aloft in the polluted cases is in part due to the lofting of cloud mass from the lower levels because no variation in vapor diffusion onto cloud droplets occurs in the highest cloud tops, as seen in figure 4.15.

4.6.2 LATENT HEAT RELEASE - FREEZING

In discussing latent heat release, the discussion of the riming of cloud water is also necessary. Figure 4.16 is a vertical profile of the average latent heat release due to riming of cloud water (referred to as LHR-RIME) and subsequent freezing.

The first point to note is that these rates are much less in magnitude than LHR-VAP. LHR-VAP is not only larger than the response seen in LHR-RIME, but it is due to cloud processes dominating over nucleation of ice and vapor diffusion onto ice as shown previously. Hence, a comparison of the rates due to cloud water and ice involved in LHR-VAP and LHR-RIME show a dominance of the role played by cloud water in convective invigoration that may be occurring due to latent heat release. This is due to the thermodynamic phase change of vapor to liquid and solid versus liquid to solid. As vapor becomes a liquid and then a solid phase, the phase change conversion releases more latent heat than simply converting from liquid to solid.

This dominance of cloud water over ice is very important in comparing this study to previous studies. It has been hypothesized that once convection reaches the freezing level, latent heat release due to freezing is linked to convective invigoration (Khain et al. 2005 and others). However, in these clouds there is not yet enough production of ice to compensate for this decrease in LHR-VAP in the higher altitudes, as seen in the previous figures and comparing LHR-VAP to LHR-RIME. This lack of ice production has impacts on the overall buoyancy of the cloud due to latent heat release and impacts the dynamics of these cumulus congestus clouds when compared to other w-momentum forcings.

When examining the trends in LHR-RIME above the freezing level, there appears to be no trend in the latent heat release due to riming with increasing CCN concentration. This could be due to one hydrometeor species dominating the response and as confirmed in the comparison of riming by ice species in section 4.5, this is due to hail. Also included in the LHR-RIME variable is the occurrence of

melting, which occurs below the freezing level. Overall, the melting of all ice hydrometeors is complete by 3 km in height, ~ 1.6 km below the freezing level (figure 4.14). Increased melting (and resultant cooling) occurs due to more ice mass formed in these congestus clouds in the more polluted cases.

4.6.3 CONDENSATE LOADING

Contributions to the w-momentum equation not only include the impact of latent heat release as discussed above, but also the impact of condensate loading. Condensate loading exerts a drag on the updraft, thus exerting a negative effect on updraft strength. This occurs in opposition to buoyancy due to latent heat release. As we saw in figure 4.8, increasing CCN concentration resulted in an increase in the total condensate found in these clouds aloft. When vertically integrated over the depth of cloud (figure 4.17), this results in increased total liquid water in the more polluted congestus clouds. The total condensate is primarily composed of cloud water aloft.

However, in the lower portion of the cloud, the latent heat release due to the formation of cloud water is largest. This latent heat produces buoyancy in the 2 to 3 km portion of cloud up to near the freezing level. At this point, there is a drop off in latent heat release due to vaporization and a lack of compensating increase in latent heat release due to riming and other ice formation. This results in the increased importance of the negative effect of condensation loading on buoyancy.

The results of this are seen in the updraft speeds of these cumulus congestus clouds previously discussed (figure 4.4). Increased updraft speeds in the more polluted scenarios resulted in an increase in the updraft speeds in the lower

portions of the clouds. This along with the increase in cloud water mass resulted in greater condensate lofting, however this condensate also exerts a greater drag. A relatively small increase in ice mass compared to cloud water occurs and this results in a very small rate of latent heat release due to freezing. Due to the lack of a new latent heat source in the upper levels and a greater condensate drag, buoyancy of these clouds is reduced resulting in a decrease in upper level updraft speeds in the more polluted cases.

4.7 COLD POOLS

Impacting the lowest level invigoration of cloud is the formation of cold pools. Cold pools form by the melting of ice hydrometeors and evaporation of precipitation below cloud base. In the cumulus congestus clouds found in this study, less rain mass was found in the more polluted cases. This means less rain is available for evaporation and absorption of latent heat. Also there is an increase in the mean size of the raindrops in the polluted cases, which also decreases evaporation rates. Knowing this, it is likely that the coldest cold pools would occur in the cleanest aerosol cases as seen in previous studies (Storer et al. 2011). This is confirmed in an evaluation of the temperature below cloud base (1 km) in figure 4.18. Hence, it is shown that in the more polluted cases that warmer, weaker cold pools occur. Variations in the forming of the cold pools, although not examined here, might also contribute to the variations in updraft speed.

Table 4.1: General changes to the hydrometeor species in the more polluted scenario. (+) indicates an increase and (–) indicates a decrease.

	Mixing Ratio	Number Concentration	Mean Diameter
Cloud Droplet	+	+	-
Raindrop	-	-	+
Pristine Ice	-	-	+
Snow	+	+	-
Aggregate	+	+	-
Graupel Aloft	-	-	+
Graupel Lower	+	+	-
Hail	-	-	+

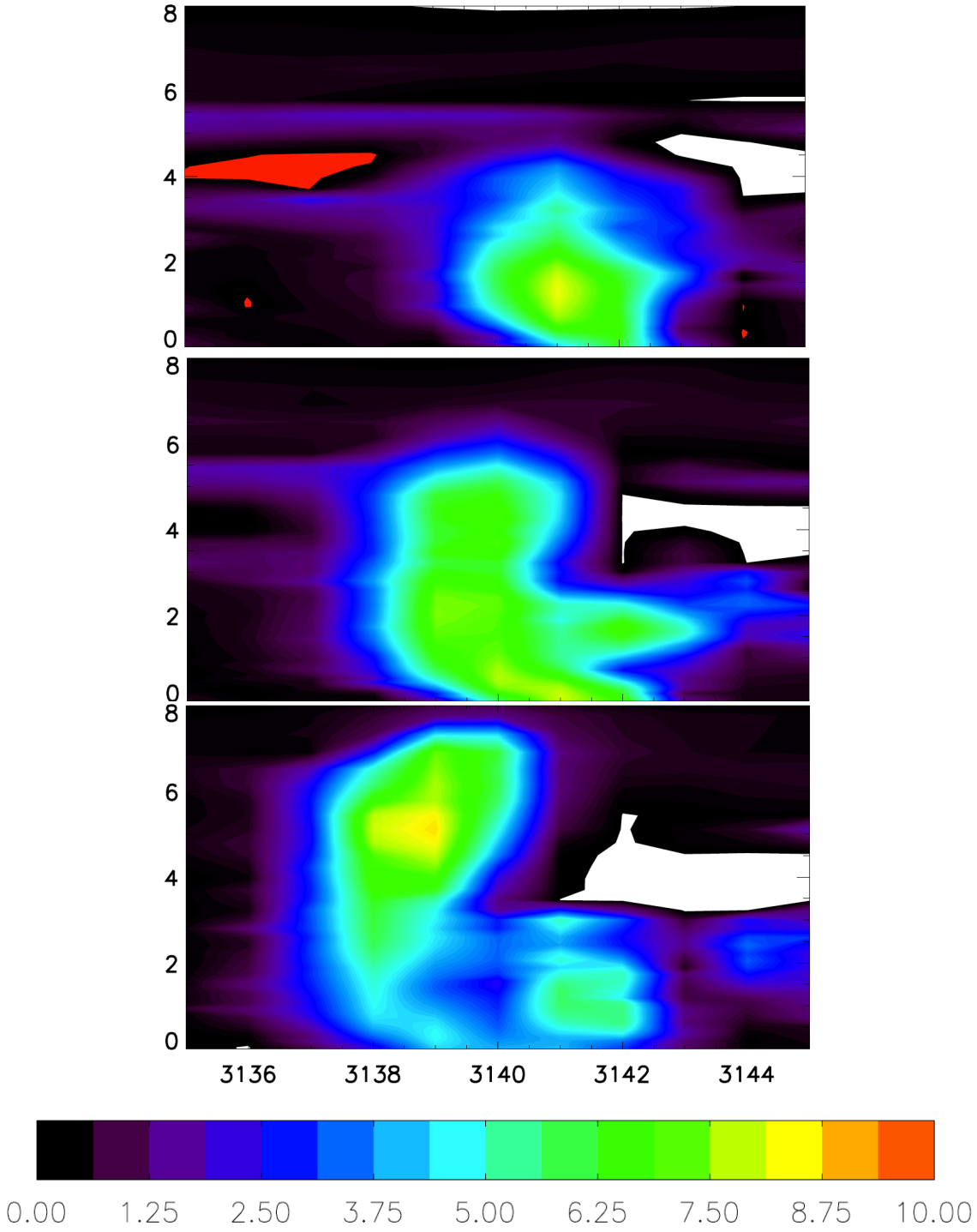

Figure 4.1: A single cumulus congestus cloud within the CCN-400 simulations, shading is total condensate (g kg^{-1}). Top panel: 15 minutes into congestus lifetime. Middle panel: 20 minutes into congestus lifetime. Bottom: 25 minutes into congestus lifetime.

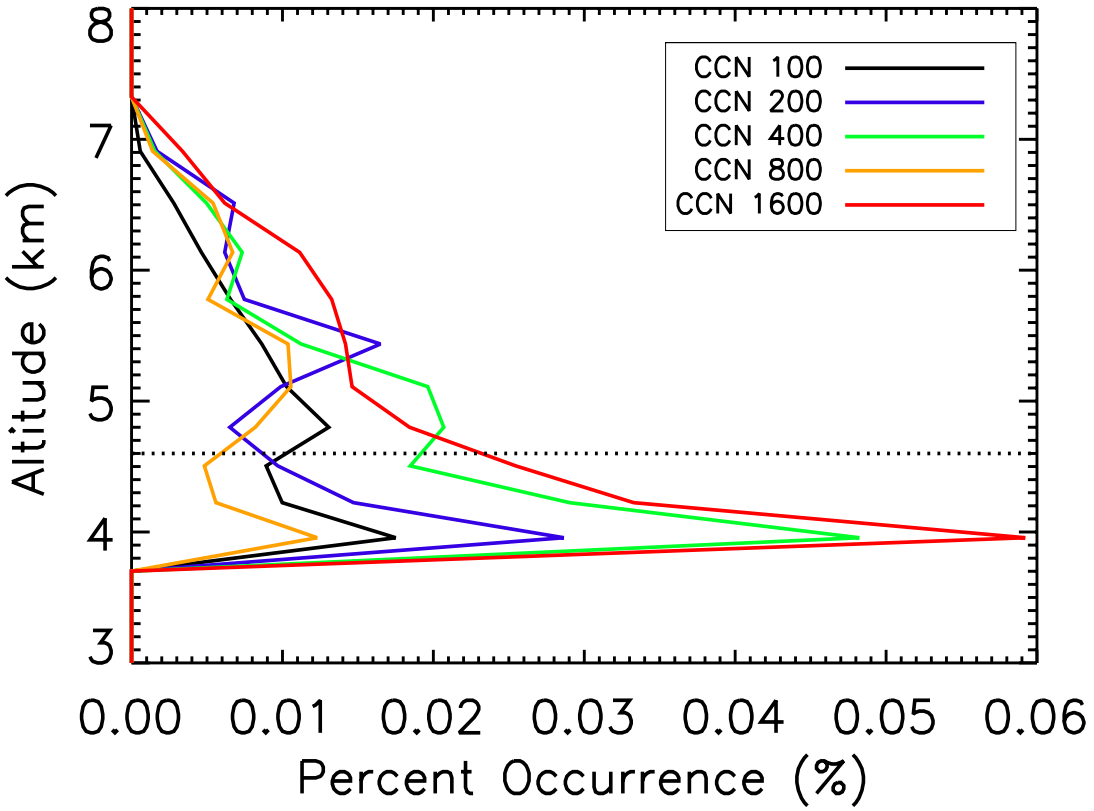

Figure 4.2: Average percent of the domain covered by cumulus congestus cloud tops, plotted by cloud top height for varying CCN concentrations. Restrictions are clouds with bases below 2 km and tops between 4 and 7 km for 10 days of simulation. Dashed line indicates the freezing level of 4.6 km.

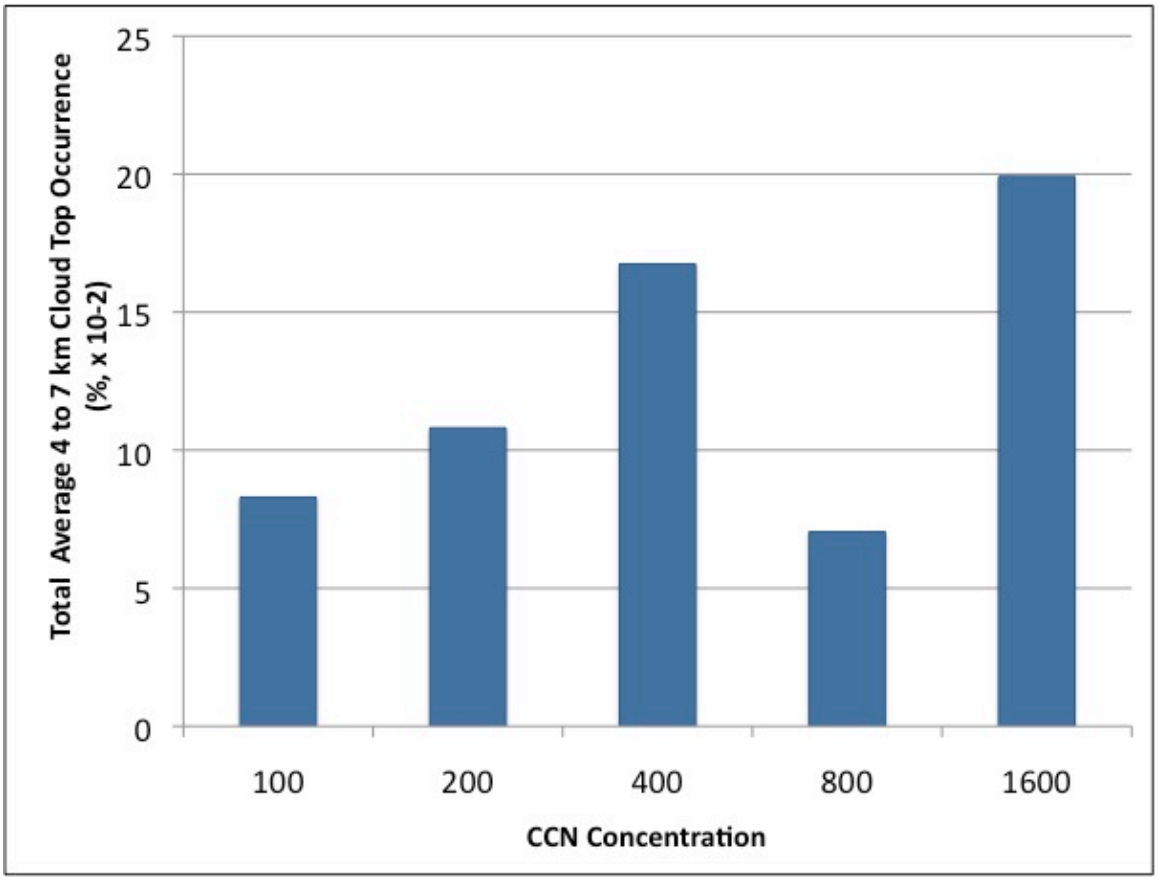

Figure 4.3: Bar graph of the total average percent of the domain covered by cumulus congestus cloud tops at 4 to 7 km altitudes AGL for varying CCN concentration.

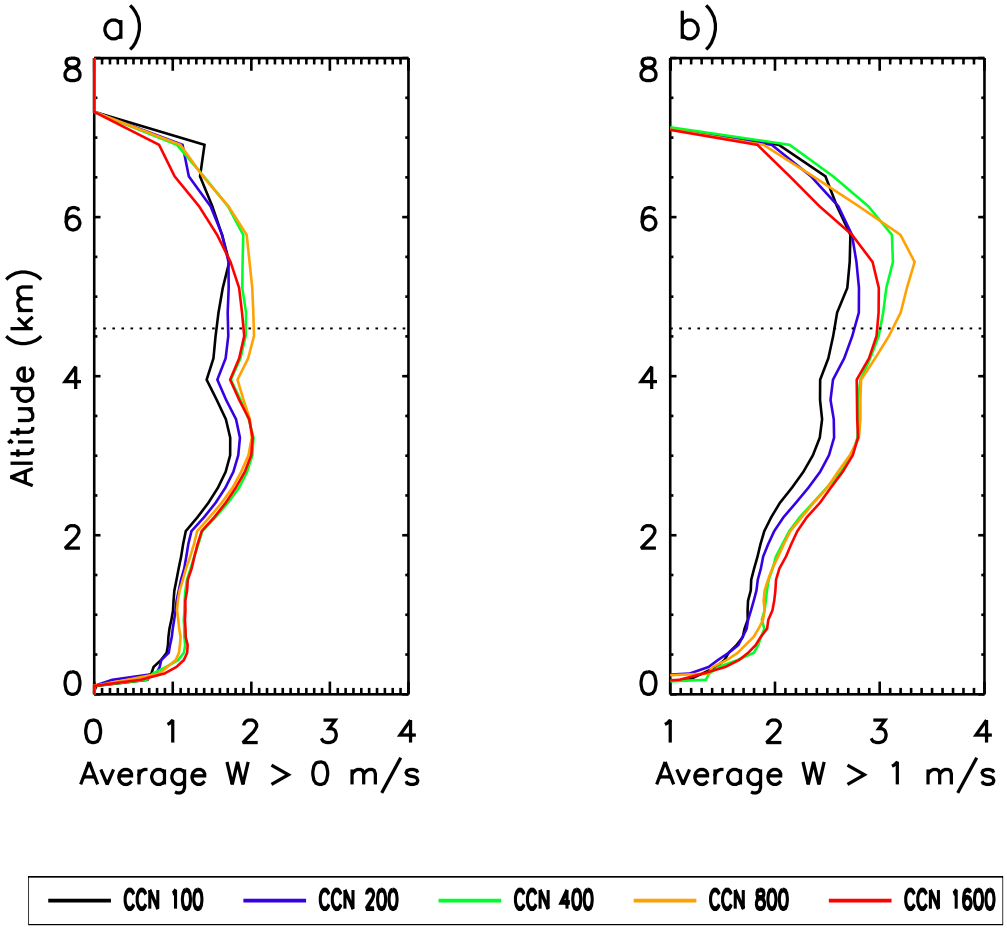

Figure 4.4: Vertical profiles of the time- and domain-averaged vertical velocities greater than (a) 0 m s^{-1} and (b) 1 m s^{-1} for varying CCN number concentrations. The dashed line indicates the freezing level.

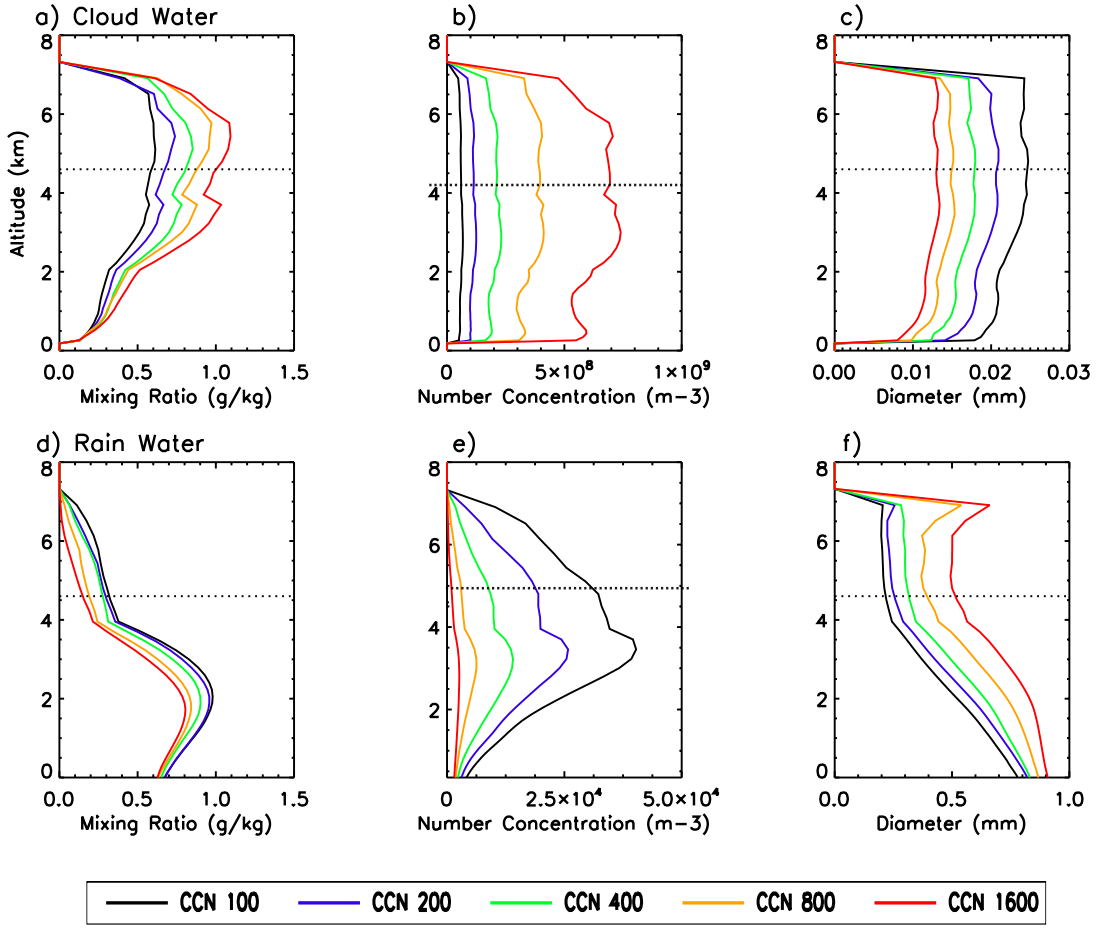

Figure 4.5: Same as figure 4.4, except for (a) cloud water mixing ratio (g kg^{-1}), (b) cloud droplet number concentration, (m^{-3}), and (c) cloud droplet mean diameter (mm) and (d) rain mixing ratio (g kg^{-1}), (e) rain number concentration (m^{-3}), and (f) rain mean diameter (mm) values..

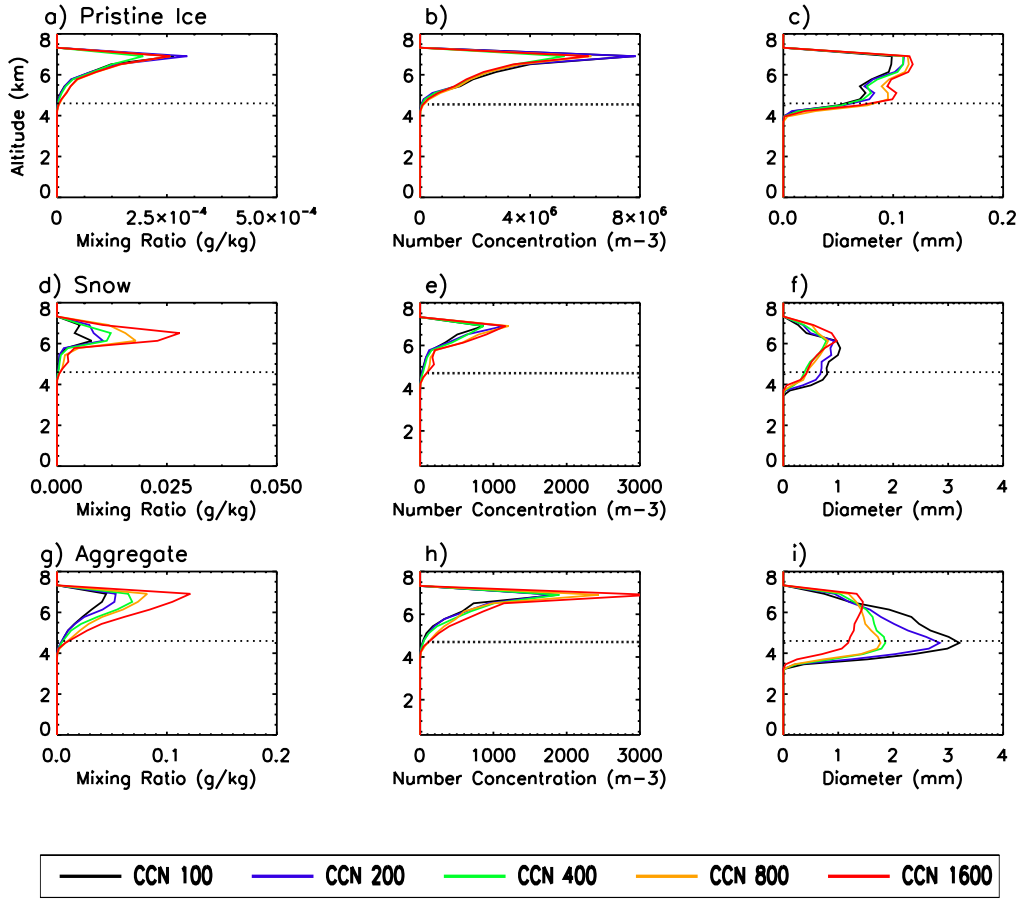

Figure 4.6: Same as figure 4.4, except for pristine ice (a) mixing ratio (g kg^{-1}), (b) number concentration, (m^{-3}), and (c) diameter (mm), snow (d) mixing ratio (g kg^{-1}), (e) number concentration (m^{-3}), and (f) diameter (mm), and aggregate (g) mixing ratio (g kg^{-1}),(h) number concentration, (m^{-3}),and (i) diameter (mm).

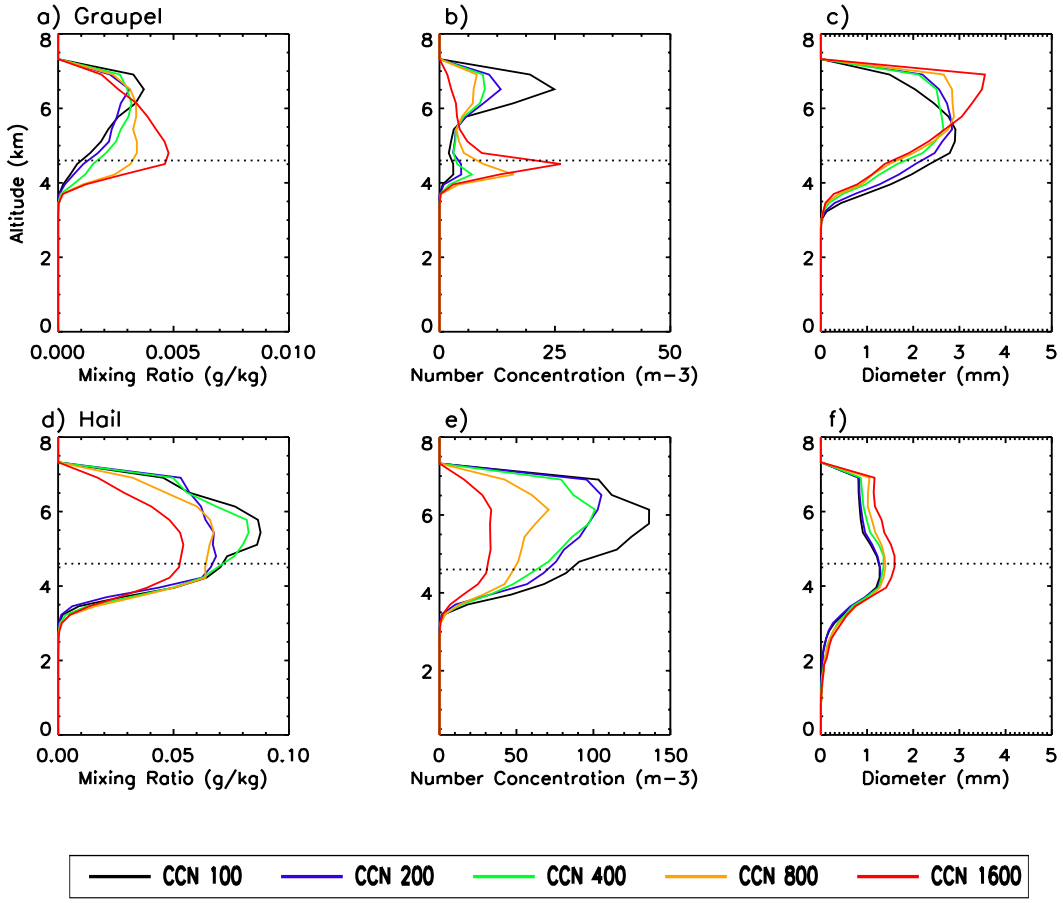

Figure 4.7: Same as figure 4.4, except for graupel (a) mixing ratio (g kg^{-1}), (b) number concentration, (m^{-3}),and (c) diameter (mm) and hail (d) mixing ratio (g kg^{-1}), (e) number concentration (m^{-3}), and (f) diameter (mm).

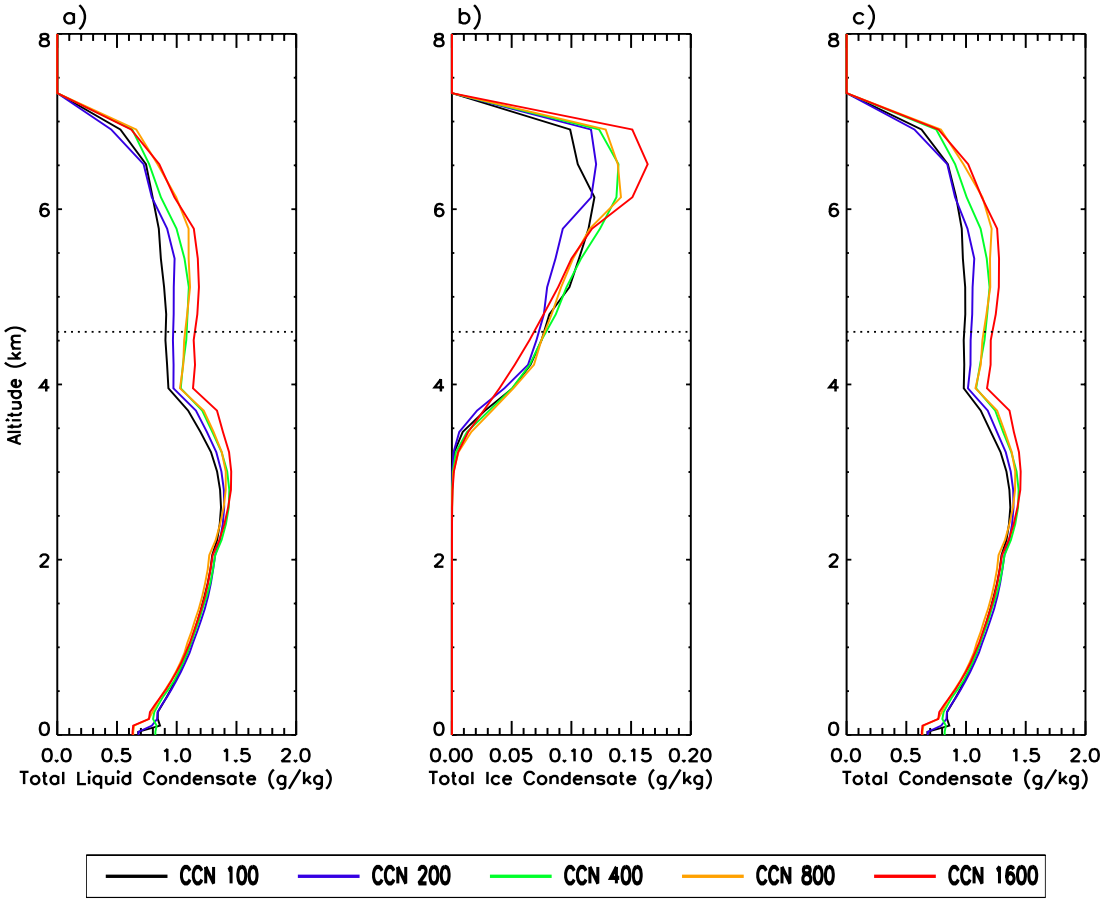

Figure 4.8: Same as figure 4.4, except for total mixing ratio (g kg^{-1}) of (a) total liquid condensate, (b) total ice condensate, and (c) total condensate (liquid + ice).

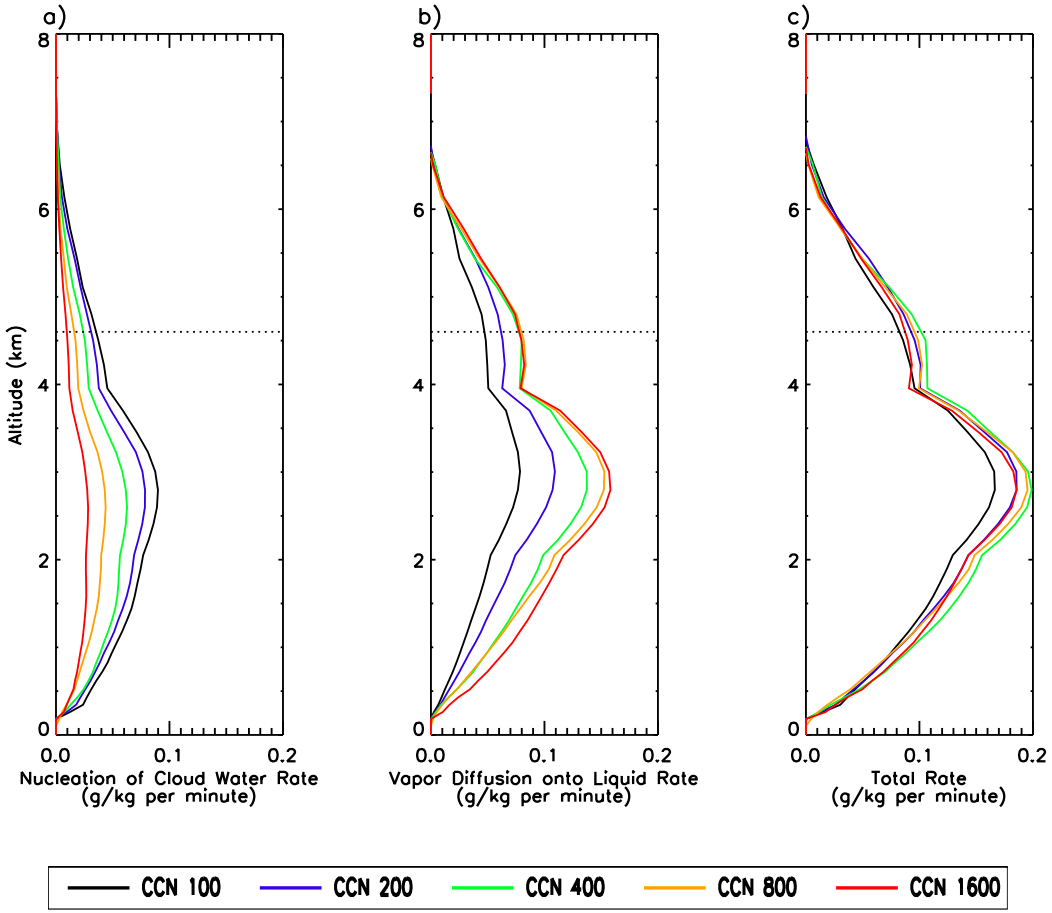

Figure 4.9: Same asfigure 4.4, but for the rate (g kg^{-1} minute^{-1}) of the (a) nucleation of cloud water, (b) vapor diffusion onto cloud, and (c) total of a and b.

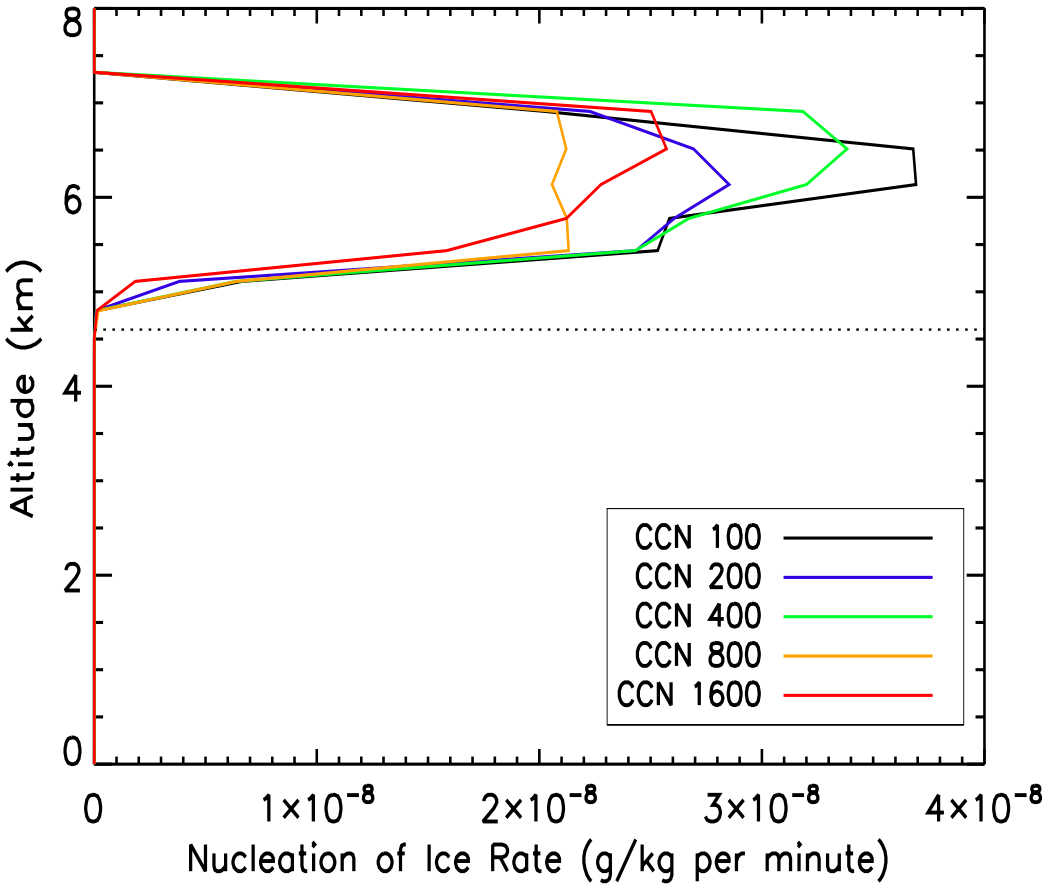

Figure 4.10: Same as figure 4.4, but for the rate of nucleation of pristine ice (g kg^{-1} $minute^{-1}$).

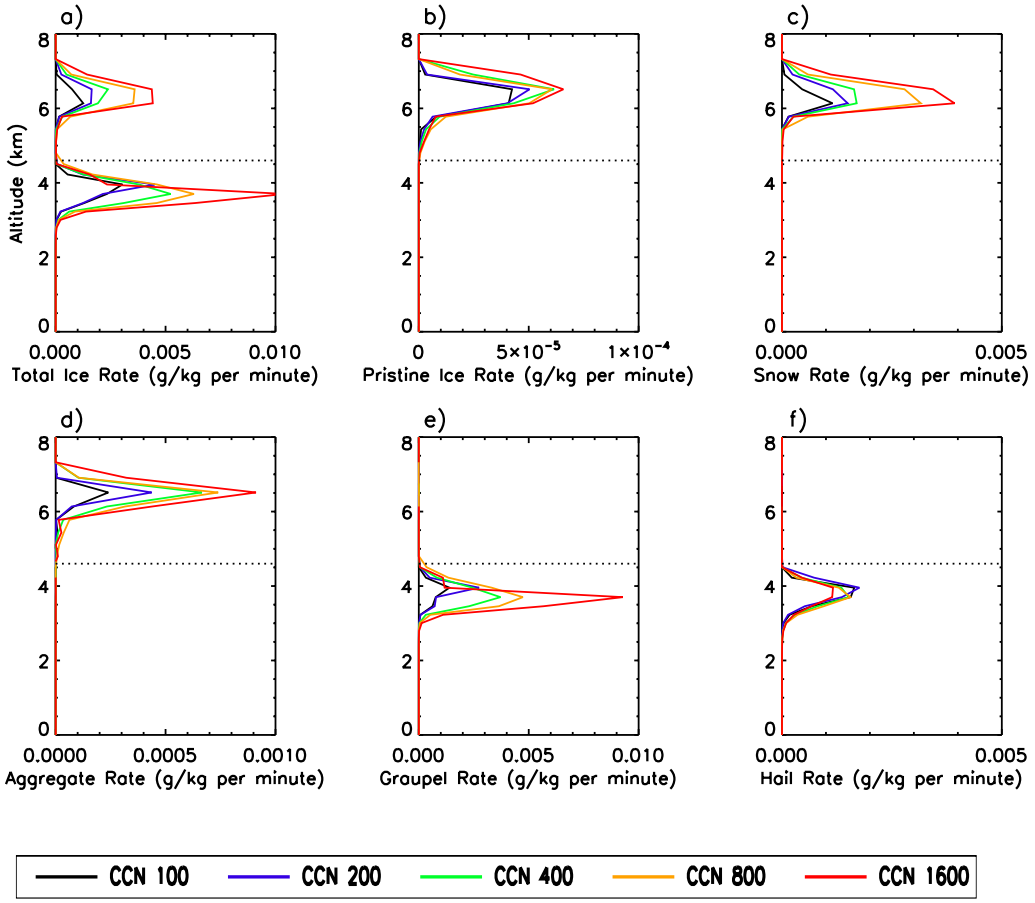

Figure 4.11: Same as figure 4.4, but for rate of vapor diffusion (g kg-^{1} minute^{-1}) onto (a) total ice,(b) pristine ice, (c) snow, (d) aggregate, (e) graupel, and (f) hail.

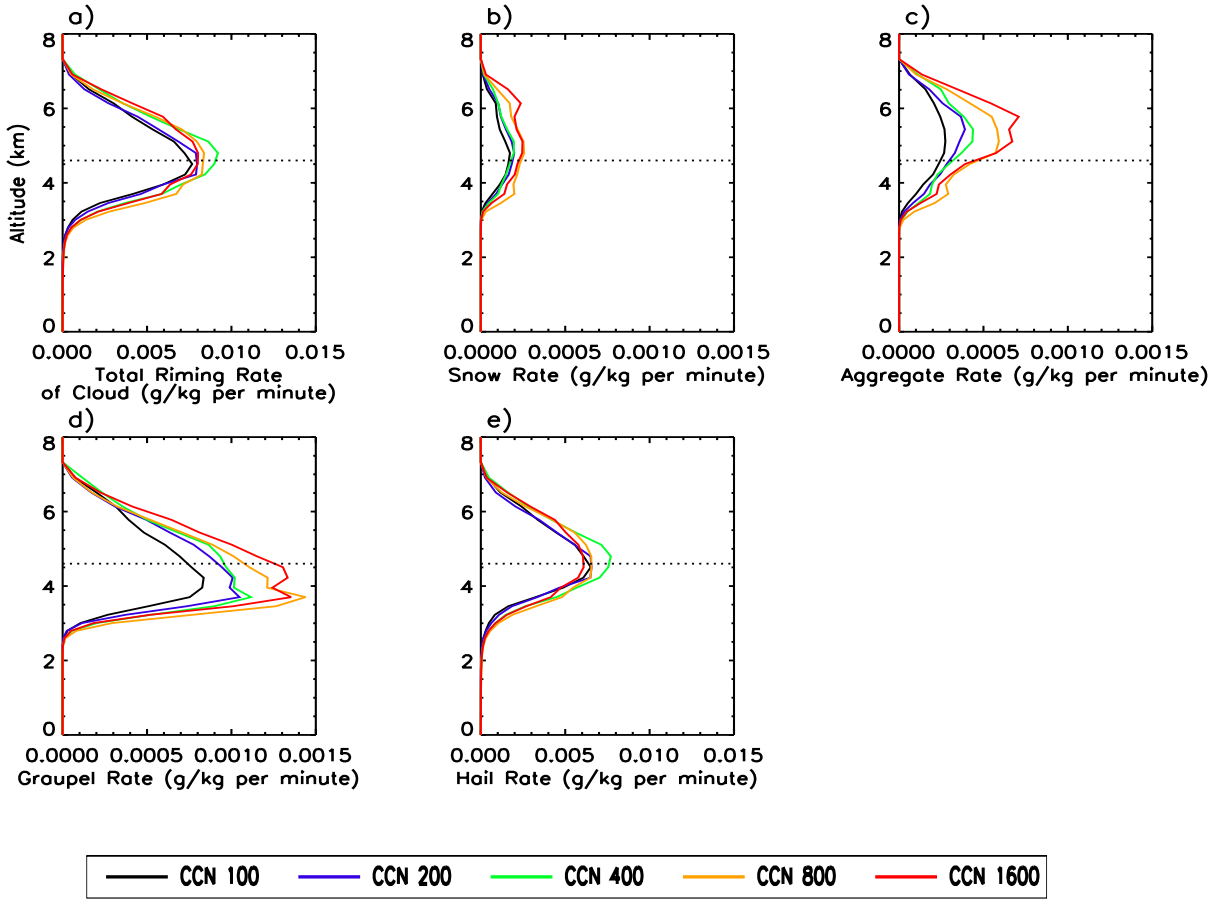

Figure 4.12: Same as figure 4.4 but for the rate of riming (g kg^{-1} minute^{-1}) of cloud water by (a) total ice, (b) snow, (c) aggregates, (d) graupel, and (e) hail.

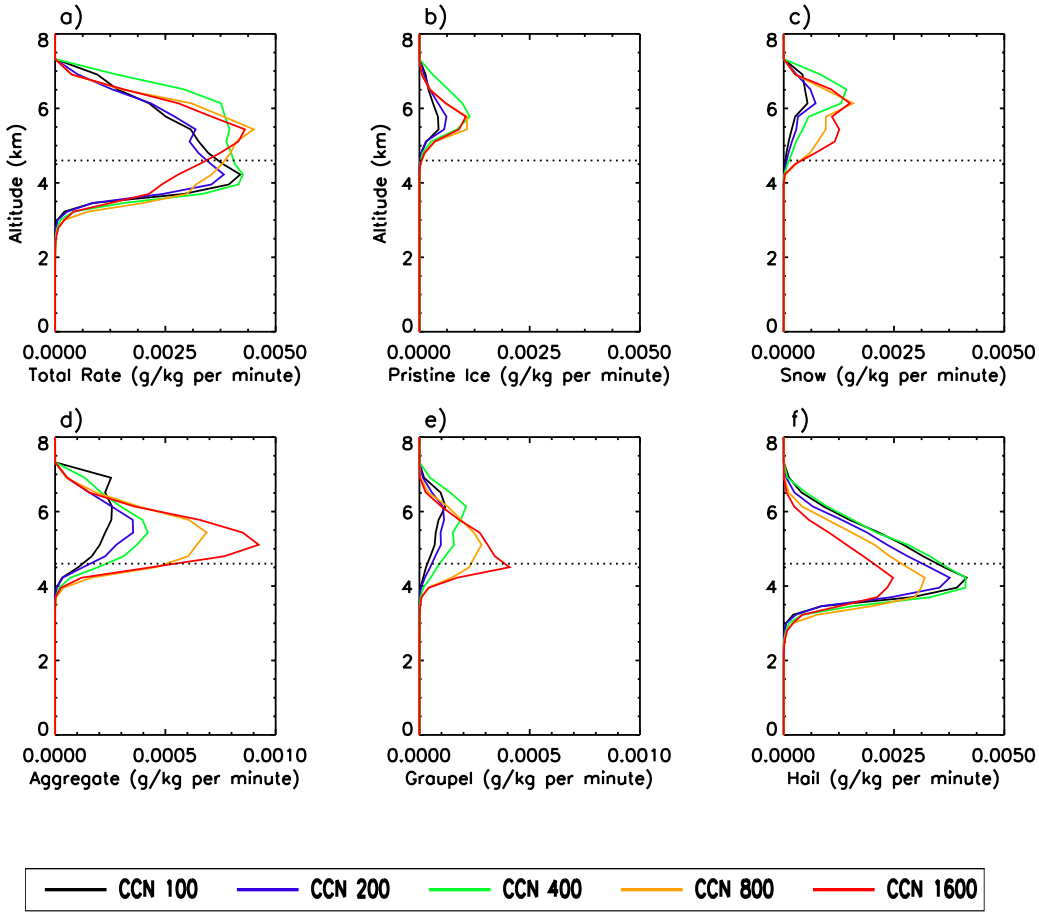

Figure 4.13: Same as figure 4.4, but for rate of riming of rain (g kg^{-1} minute^{-1}) by (a) all ice species, (b) pristine ice, (c) snow, (d) aggregates, (e) graupel, and (f) hail.

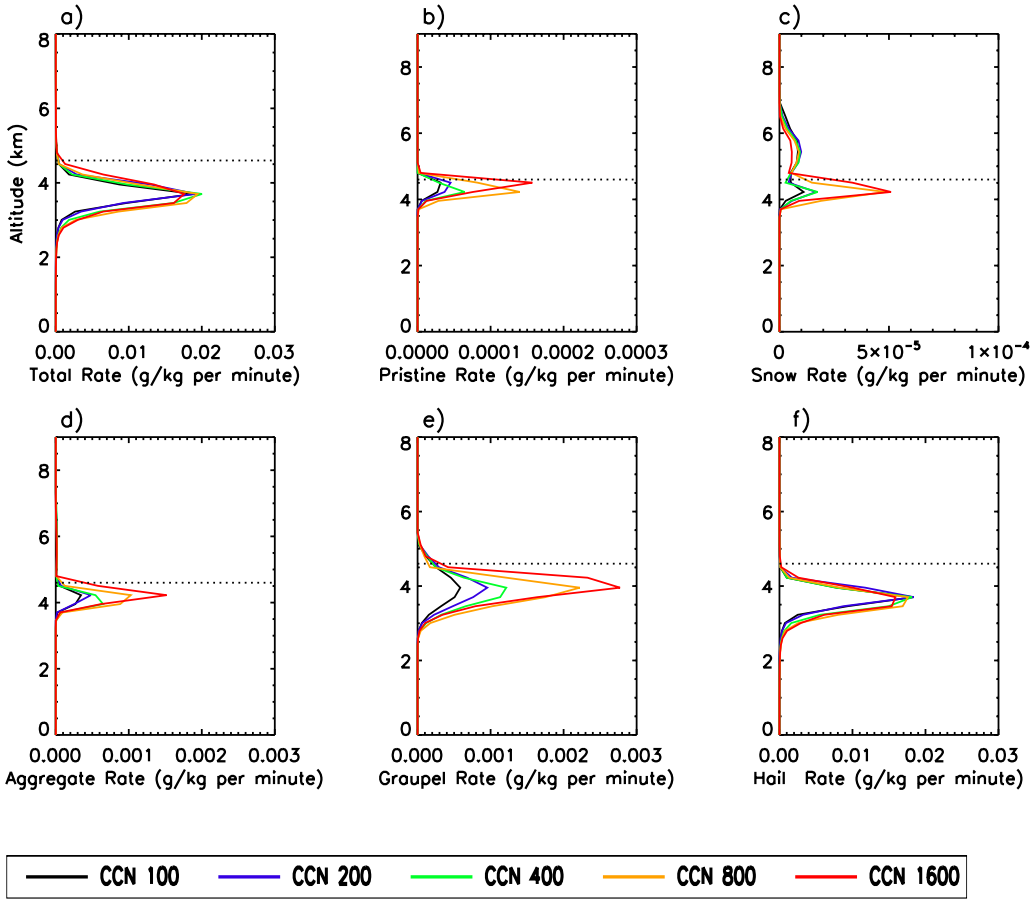

Figure 4.14: Same as figure 4.4, but for rate of melting of (g kg^{-1} $minute^{-1}$) (a) total ice, (b) pristine ice, (c) snow, (d) aggregates, (e) graupel, and (f) hail.

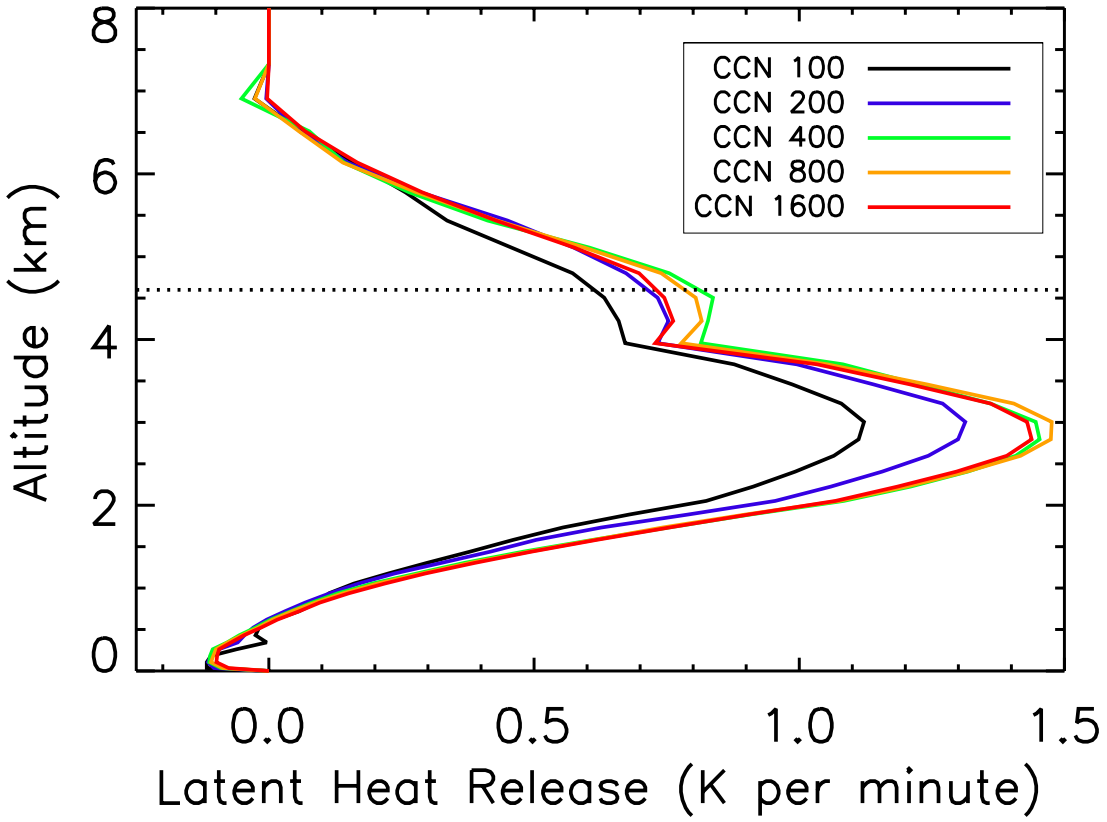

Figure 4.15: Same as figure 4.4, except for latent heat rates due to vapor diffusion onto droplets and ice, and nucleation of droplets and ice (K minute^{-1}).

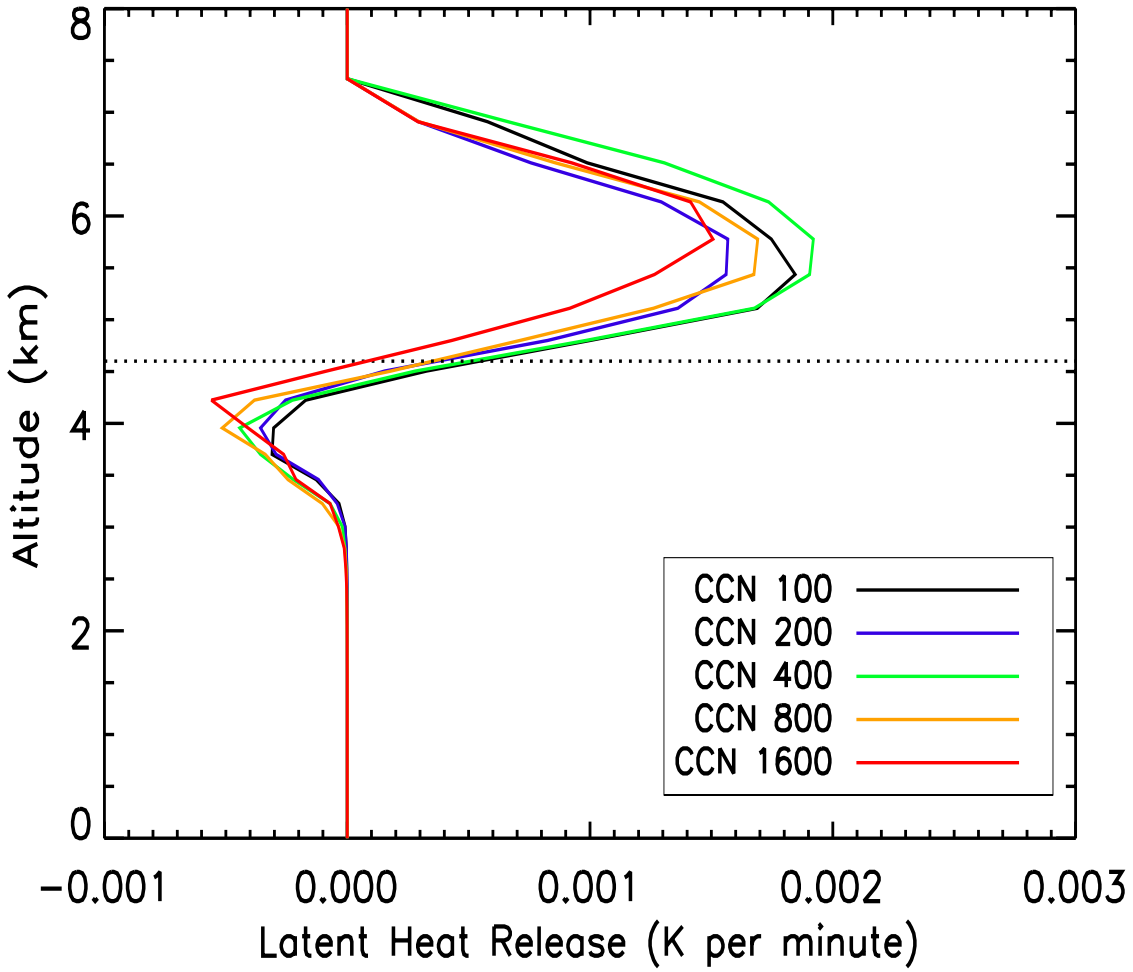

Figure 4.16: Same as figure 4.4, but for latent heat rates due to the riming of cloud water (K minute^{-1}).

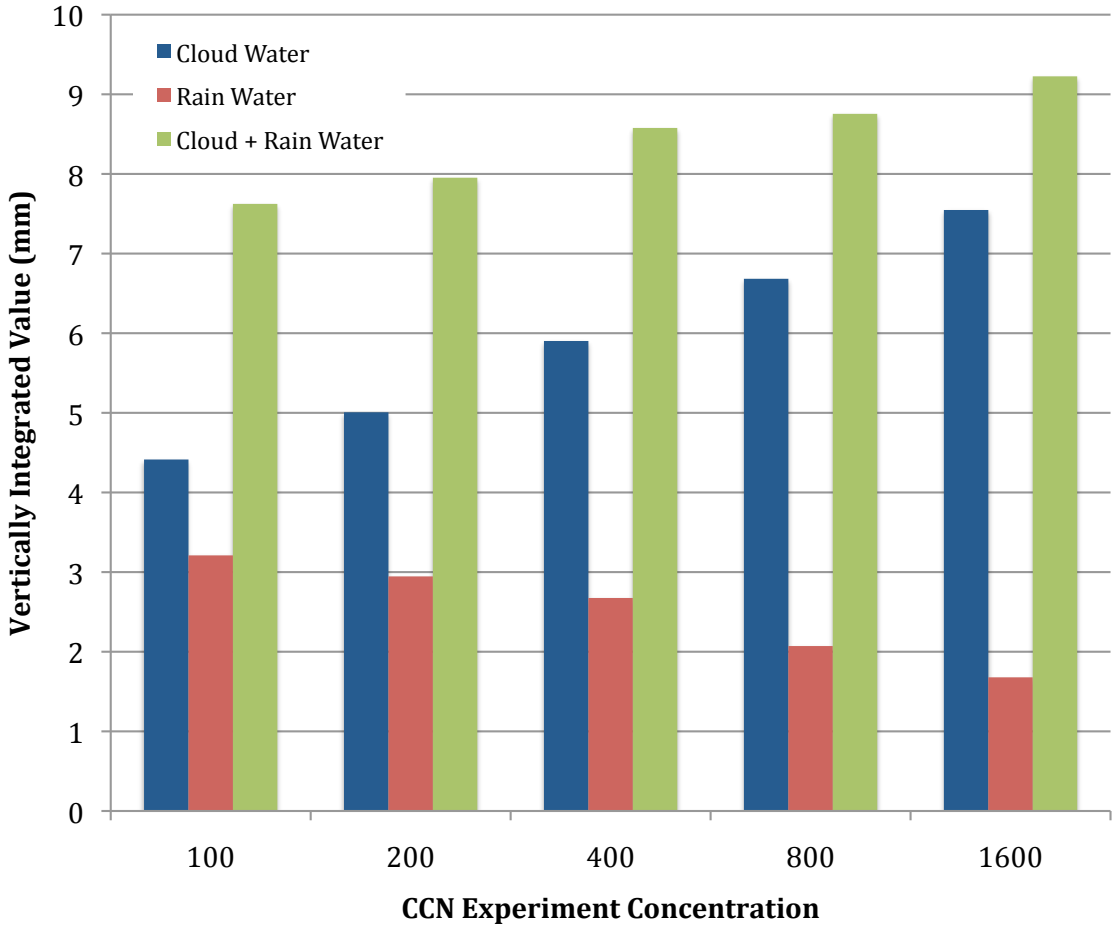

Figure 4.17: Vertically integrated value (mm) of horizontally and temporally averaged in-cloud cloud water, rain water, and total liquid water as a function of CCN.

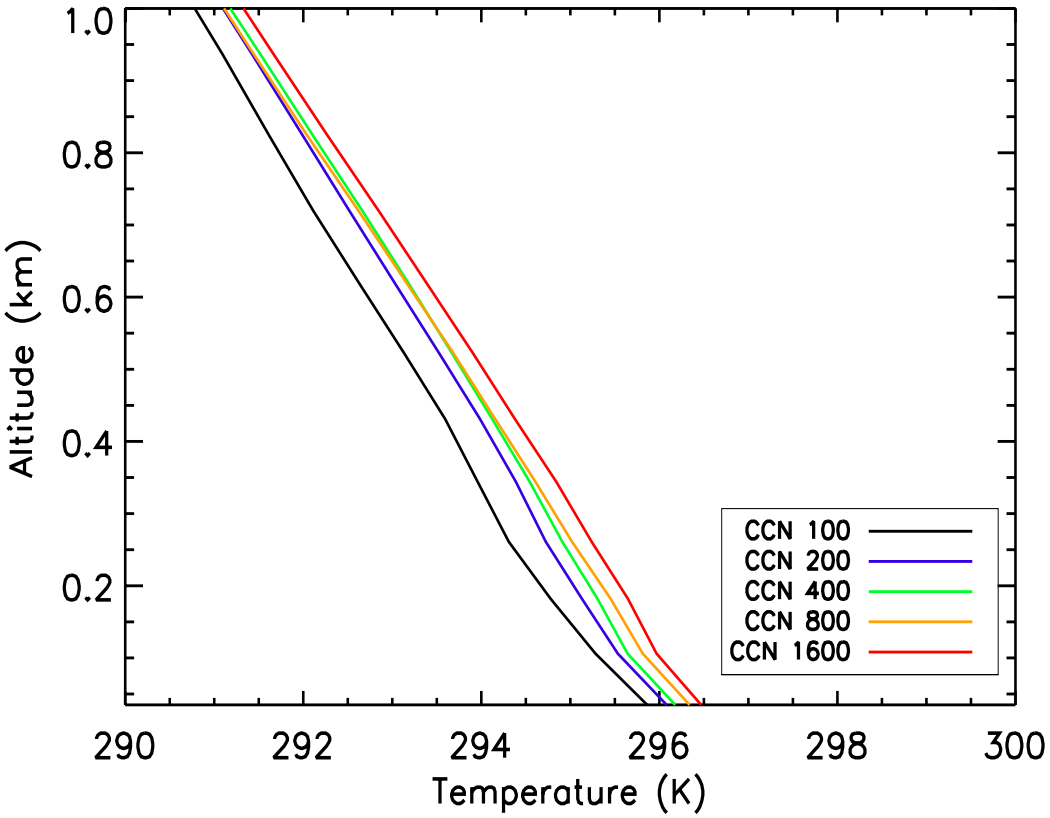

Figure 4.18: Same as figure 4.4, except for the average temperature under cumulus congestus clouds.

5. CONCLUSION

The impact of clouds on climate is a problem yet to be solved and the inclusion of aerosol indirect forcing is hypothesized to be important in this solution (Solomon et al. 2007). The importance of aerosol-cloud interactions is heavily based on cloud type (Seifert and Beheng, 2006, vdH2011) and thus an evaluation of a particular cloud regime response is important. The cloud type examined here are cumulus congestus clouds, a component of the trimodal distribution of tropical convection (Johnson et al. 1999).

Cumulus congestus clouds are mid-level clouds whose development is based on the weak stable layer present at the freezing level (Johnson et al. 1999, Redelsperger et al. 2002, Takemi et al. 2004, Jensen and Del Genio 2006, Haynes and Stephens 2007). They evolve from trade wind cumulus clouds and may possibly transition into deep convection or remain terminal (Luo et al. 2009). These clouds serve to moisten the middle troposphere and contribute significantly to precipitation to the tropics (Johnson et al. 1999, Haynes and Stephens 2007). Any changes in the characteristics of cumulus congestus clouds due to aerosol forcing would thus have an impact on the trimodal convection characteristics commonly observed in the tropics.

Simulations using an advanced cloud-resolving model (RAMS) with a bin-emulating two-moment bulk scheme, demonstrate that cumulus congestus clouds in

a tropical disturbed region are impacted by the presence of an advecting aerosol layer. This idealized scenario is not unlike the occurrences of a Saharan or Asian dust layer being transported over the Atlantic or Pacific oceans. Increased aerosols serving as CCN resulted in more numerous, smaller cloud droplets (Albrecht 1989). This change in the drop size distribution, and the subsequent impacts of enhanced aerosol concentrations on congestus cloud processes are shown in a schematic, figure 5.1. In process 1, an increase in cloud water mass in more polluted conditions was produced due to the suppression of warm rain processes through the change in droplet size and number concentration. Due to the increased surface area of these more numerous, although smaller cloud droplets, they were able to grow further through vapor diffusional growth that occurred at the expense of the nucleation of new droplets (process 2). Both nucleation of cloud droplets and vapor diffusion onto these droplets result in the release of latent heat. Latent heating rates were greatest below the freezing level and in the more polluted cases. The vapor diffusion onto cloud droplets was found to be the largest factor in the making of latent heat available to the cloud and the subsequent impacts on buoyancy and updraft speed in the more polluted cases. This increased updraft speed (process 3) resulted in more frequent, higher cloud tops near and above the freezing level (process 4b).

The greater amount of available cloud water in the polluted cases is then lofted into upper levels of cloud by the stronger updrafts and made available for freezing (process 4a). In the more polluted conditions, greater ice condensate was observed to occur. However, the ice mass created in these congestus clouds and its

associated rate of latent heat release is found to be relatively small compared to that released by warm phase processes. Though increased cloud top frequency occurs above the freezing level compared to the clean case, any further invigoration of these clouds above the freezing level is limited by the relatively low amounts of ice produced, and is offset to some degree by the larger amounts of cloud water produced in the more polluted cases. A decrease in the updraft trend with increasing CCN concentration occurred above the freezing level. Even though this decrease occurs, the increase in buoyancy near and below the freezing level works to create not only more clouds below 4 km, but also above the freezing level through the lofting of cloud water.

This study's results are of importance in the determination of the effects not only of aerosols on cumulus congestus clouds, but also of what processes govern their growth. Congestus clouds in this study appear to be strongly controlled by latent heat release due to vapor diffusional growth of cloud droplets. The convective invigoration above the freezing level was limited by the lack of ice formation, as previously hypothesized in Johnson et al. (1999) and Zuidema (1998). They stated that a lack of ice could occur as high as 1 to 2 km above the freezing level, which was similar to what was observed for these clouds. In order for these clouds to become deeper convection, these clouds would need to enhance their buoyancy through further glaciation.

Previous studies have found that increased aerosols serving as CCN resulted in convective invigoration of deep convection due to increased latent heat release through freezing (Andreae et al. 2004, Khain et al. 2005, van den Heever et al. 2006).

This invigoration may result in increased precipitation after a delay in the formation processes during the warm cloud phase. Congestus have previously been hypothesized to be restricted in their growth until production of buoyancy from freezing (Johnson et al. 1999). Here it has been found that diffusional growth processes are important in the initial vertical development of congestus through stronger updrafts and subsequent enhanced lofting of cloud water. Ice amounts are relatively small, and the contributions to buoyancy enhancements from ice formation are less significant. However, this study focused only on the cumulus congestus clouds phase and thus has not determined the impacts of aerosols on these clouds as they potentially transition to deeper convection. This evaluation of cumulus congestus clouds to deeper convection is an area of continuing research.

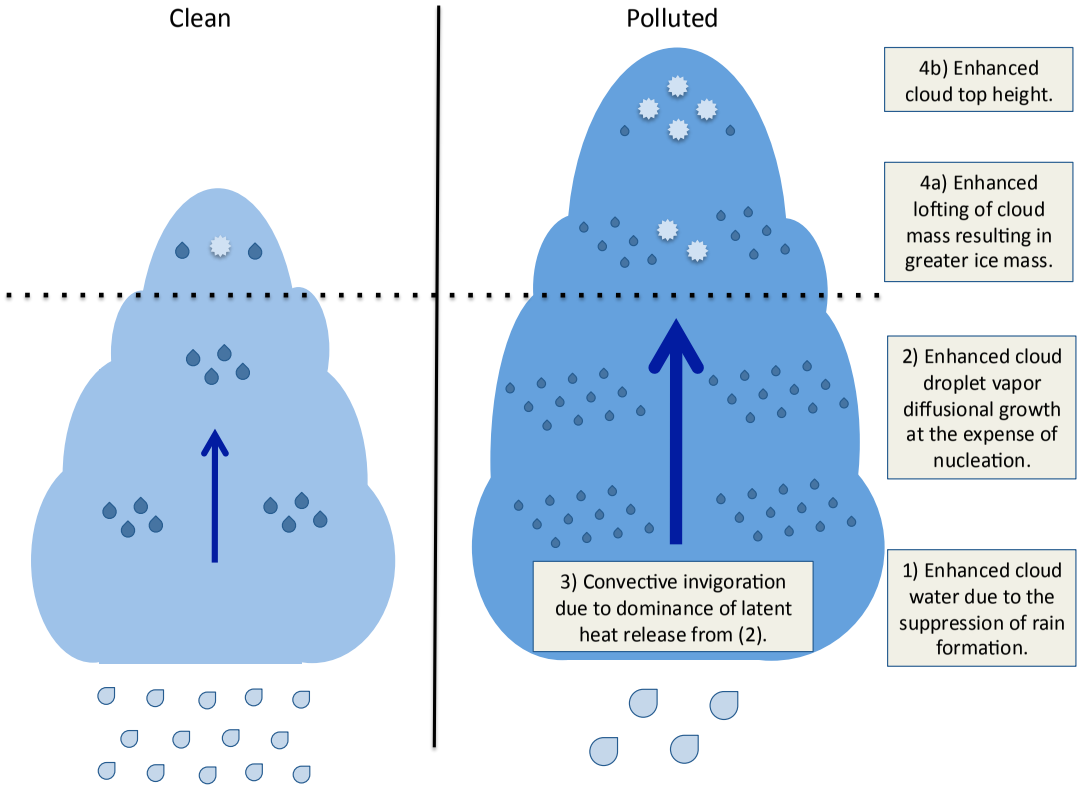

Figure 5.1: A schematic of the processes important to cumulus congestus clouds observed in the clean versus polluted environment. Process description is located in chapter 5.

6. REFERENCES

Albrecht, B., 1989: Aerosols, cloud microphysics, and fractional cloudiness. *Science*, **245**, 1227-1230.

Arakawa, A., 2004: The cumulus parameterization problem: Past, present and future. *J. Climate*,**17**, 2493-2525.

Berg, W., T. L'Ecuyer, and S. C. van den Heever, 2008: Evidence for the impact of aerosols on the onset and microphysical properties of rainfall from a combination of satellite observations and cloud-resolving model simulations. *J. Geophys. Res.* **113**, D14S23, doi:10.1029/2007JD009649.

Cotton, W.R., R.A. Pielke Sr., R.L. Walko, G.E. Liston, C.J. Tremback, H. Jiang, R.L. McAnelly, J.Y. Harrington, M.E. Nicholls, G.G. Carrio, and J.P. McFadden, 2003: RAMS2001: Current status and future directions. *Meteor. Atmos. Phys*., **82**, 5-29.

Cziczo, D. J., Murphy, D. M., Hudson, P. K., and Thomson, D. S.: Single particle measurements of the chemical composition of cirrus ice residue during CRYSTAL-FACE, *J. Geophys. Res*., **109(D4),** D04201, doi:10.1029/2003JD004032, 2004.

DeMott, P. J., Sassen, K., Poellot, M. R., Baumgardner, D., Rogers, D. C., Brooks, S. D., Prenni, A. J., and Kreidenweis, S. M.: African dust aerosols as atmospheric ice nuclei *Geophys. Res. Lett.,* **30(14),** 1732, doi:10.1029/2003GL017410, 2003.

Feingold, G., and A. J. Heymsfield, 1992: Parameterizations of condensational growth of droplets for use in general circulation models. *J. Atmos. Sci*., **49**, 2325-2342.

Field, P. R., O. Mohler, P. Connolly, M. Kramer, R. Cotton, A. J. Heymsfield, H. Saathoff, and M. Schnaiter, 2006: Some ice nucleation characteristics of Asian and Saharan desert dust. *Atmos. Chem. Phys.*, **6**, 2991-3006.

Glossary of Meteorology. 2011. American Meteorological Society. < http://amsglossary.allenpress.com/glossary>

Grabowski, W.W., 2006: Indirect impact of atmospheric aerosols in idealized simulations of convective-radiative quasi equilibrium. *J. Climate*, **19**, 4664-4682.

Harrington, J.Y., 1997: The effects of radiative and microphysical processes on simulated warm and transition season Arctic stratus. Ph.D. dissertation, Colorado State University, 289pp. [Available from Department of Atmopsheric Science, Colorado State University, Fort Collins, CO 80523.]

Hartmann, D. L., 1994: *Global Physical Climatology.* Academic Press, 411 pp.

Haynes, J. M., and G. L. Stephens, 2007: Tropical oceanic cloudiness and the incidence of precipitation: Early results from CloudSat. *Geophys. Res. Lett.,* **34**, L09811, doi:10.1029/2007GL029335.

Heymfield, A. J., and R. M. Sabin, 1989: Cirrus crystal nucleation by homogeneous freezing of solution droplets. *J. Atmos. Sci*., **46**, 2252-2264.

- - -, C. A. Knight, and J. E. Dye, (1979): Ice inititation processes in unmixed cores in northeast Colorado cumulus congestus clouds. *J. Atmos. Sci*., **36**, 2216-2229.

Hill, G.E., 1974: Factors controlling the size and spacing of cumulus clouds as revealed by numerical experiments. *J. Atmos. Sci*., **31,** 646-673.

Hobbs, P. V, and A. L. Rangno, 1985: Ice particle concentration in cloud. *J. Atmos. Sci.*, **42**, 2523-2549.

Houghton, J.T., Y. Ding, D.J. Griggs, M. Noguer, P.J. van den Linden, and D. Xiaosu, Eds., 2001: *Climate Change 2001: The Scientific Basis*. Cambridge University Press, 944 pp.

Jensen, Michael P., Anthony D. Del Genio, 2006: Factors limiting convective cloud-top height at the arm nauru island climate research facility. *J. Climate*, **19**, 2105–2117.

Johnson, Richard H., Paul E. Ciesielski, Kenneth A. Hart, 1996: Tropical inversions near the 0°c level. *J. Atmos. Sci.*, **53**, 1838–1855.

- - -, T.M. Rickenbach, S.A. Rutledge, P.E. Ciesielski, and W.H. Schubert, 1999: Trimodal characteristics of tropical convection. *J. Climate*, **12**, 2397-2418.

Kessler, E., 1969: *On the Distribution and Continuity of Water Substance in Atmospheric Circulation. Meteor. Monogr*., No. 32, Amer. Meteor. Soc., 84pp.

Khain, A., D. Rosenfeld, and A. Pokrovsky, 2005: Aerosol impact on the dynamics and microphysics of deep convective clouds. *Q. J. R. Meteorol. Soc*., **131**, 2639-2663.

- - -, N. BenMoshe, and A. Pokrovsky, 2008: Factors determining the impact of aerosols on surface precipitation from clouds: An attempt at classification. *J. Atmos. Sci*., **65**, 1721-1748.

Kiehl, J.T., and K.E. Trenberth, 1997: Earth's annual global mean energy budget. *Bull. Amer. Meteor. Soc*., **78**, 197-208.

Lau, K. M., and H. T. Wu, Warm rain processes over tropical oceans and climate implications, *Geophys. Res. Lett*., **30(24),** 2290, doi:10.1029/2003GL018567, 2003.

Lerach, D. G., B. J. Gaudet, and W. R. Cotton, 2008: Idealized simulations of aerosol influences on tornadogenesis. *Geophys. Res. Lett*., **35**, L23806, doi:10.1029/2008GL035617.

Lilly, D.K., 1962: On the numerical simulation of buoyant convection. *Tellus*, **14**, 148-172.

Lohmann, U. and J. Feichter, 2005: Global indirect effects: a review. *Atmos. Chem. Phys.*, **5**, 715-737.

Luo, Z., G. Liu, and G. L. Stephens, 2008: CloudSat adding new insights into tropical convection. *Geophys. Res. Lett*., **35**, L19819, doi:10.1029/2008GL035330.

Malkus, J. S., and H. Riehl, 1964: *Cloud Structure and Distributions over the Tropical Pacific Ocean.* University of California Press, 229 pp.

Mesinger, F., and A. Arakawa, 1976: Numerical methods used in atmospheric models. GARP Publication Series 14, WMO/ICSU Joint Organizing Committee, 64pp.

Meyers, M.P., R.L. Walko, J.Y. Harrington, and W.R. Cotton., 1997: New RAMS cloud microphysics parameterization. Part II: The two-moment scheme. *Atmos. Res*., **45**, 3-39.

Pielke, R.A., W.R. Cotton, R.L. Walko, C.J. Tremback, W.A. Lyons, L.D. Grasso, M.E. Nicholls, M.D. Moran, D.A. Wesley, T.J. Lee, and J.H. Copeland, 1992: A comprehensive meteorological modeling system – RAMS. *Meteor. Atmos. Phys*., **49**, 69-91.

Posselt, D.J., S.C. van den Heever, and G.L. Stephens, 2008: Trimode cloudiness and tropical stable layers at radiative convective equilibrium. *Geophys. Res. Lett.,* **35**, L08802, doi:10.1029/2007GL033029.

Prenni, A. J., P. J. DeMott, C. Twohy, M. R. Poellot, S. M. Kreidenweis, D. C. Rogers, S. D. Brooks, M. S. Richardson, and A. J. Heymsfield (2007), Examinations of ice formation processes in Florida cumuli using ice nuclei measurements of anvil ice crystal particle residues, *J. Geophys. Res.,* **112**, D10221, doi:10.1029/2006JD007549.

Prospero, J.M., and T.N. Carlson, 1981: Saharan air outbreaks over the tropical North Atlantic. *Pure Appl. Geophys*., **119**, 677-691.

- - - ,1999: Longterm measurements of the transport of African mineral dust to the Southeastern United States: Implications for regional air quality, *J. Geophys. Res*., **104** (15),917–15,927.

Pruppacher, H. R. and Klett, J. D.: Microphysics of Clouds and Precipitation, Kluwer Acad., Norwell, Mass., 1997.

Ramanathan, V., P. J. Crutzen, J. T. Kiehl, and D. Rosenfeld, 2001: Aerosols, climate, and the hydrological cycle. *Science*, **294**, 2199-2124.

Rangno, A. L, and P. V. Hobbs, 1991: Ice particle concentrations and precipitation development in small polar maritime cumuliform clouds. *Q. J. R. Meteorol. Soc.*, **117**, 207-241.

- - -, and P. V. Hobbs, 1994: Ice particle concentrations and precipitation development in small continental cumuliform clouds. *Q. J. R. Meteorol. Soc.*, **120**, 573-601.

Redelsperger, J.-L., D. B. Parsons, and F. Guichard, 2002: Recovery processes and factors limiting cloud-top height following the arrical of a dry intrusion observed dur TOGA COARE. *J. Atmos. Sci*., **59**, 2438-2457.

Riehl, H., and J.S. Malkus, 1958: On the heat balance in the equatorial trough zone. *Geophysica*, **6**, 503-538.

Rosenfeld, D., 1999: TRMM observed first direct evidence of smoke from forest fires inhibiting rainfall. *Geophys. Res. Lett*., **26**, 3105-3108.

Saleeby, S.M., and W.R. Cotton, 2004: A large-droplet mode and prognostic number concentration of cloud droplets in the Colorado State University Regional Atmospheric Modeling System (RAMS). Part I: Module descriptions and supercell test simulations*. J. Appl. Meteor***., 43**, 182-195.

- - -, - - -, D. Lowenthal, R. D. Borys, and M. A. Wetzel, 2009: Influence of Cloud Condensation Nuclei on Orographic Snowfall. *J. Appl. Meteor. Climatol.*, **48**, 903–922.

Sassen, K., Indirect climate forcing over the western US from Asian dust storms, *Geophys. Res. Lett*., **29**, doi:10.1029/2001GL014051, 2002.

- - -, P. J. DeMott, J. M. Prospero, and M. R. Poellot, Saharan dust storms and indirect aerosol effects on clouds: CRYSTAL-FACE Results, *Geophys. Res. Lett*., **30(12),** doi:10.1029/2003GL017371, 2003.

Seifert, A., and K.D. Beheng, 2006: A two-moment cloud microphysics parameterization for mixed-phase clouds. Part 2: Maritime vs continental deep convective storms. *Meteor. Atmos.Phys*., **92**, 67-82.

Smagorinsky, J., 1963: General circulation experiments with the primitive equations. I. The basic experiment. *Mon. Wea. Rev*., **91**, 99-164.

Solomon, S., D. Qin, M. Manning, R.B. Alley, T. Berntsen, N.L. Bindoff, Z. Chen, A. Chidthaisong, J.M. Gregory, G.C. Hegerl, M. Heimann, B. Hewitson, B.J. Hoskins, F. Joos, J. Jouzel, V. Kattsov, U. Lohmann, T. Matsuno, M. Molina, N. Nicholls, J. Overpeck, G. Raga, V. Ramaswamy, J. Ren, M. Rusticucci, R. Somerville, T.F. Stocker, P. Whetton, R.A. Wood and D. Wratt, 2007: Technical Summary. In: Climate Change 2007: The Physical Science Basis. Contribution of Working Group I to the Fourth Assessment Report of the Intergovernmental Panel on Climate Change [Solomon, S., D. Qin, M. Manning, Z. Chen, M. Marquis, K.B. Averyt, M. Tignor and H.L. Miller (eds.)]. Cambridge University Press, Cambridge, United Kingdom and New York, NY, USA.

Stephens, G.L., 1990: On the relationship between water vapor over the oceans and sea surface temperature. *J. Climate*, **3**, 634-645.

Storer, R. L., S. C. van den Heever, and G. L. Stephens, 2010: Modeling aerosol impacts on convective storms in different environments. *J. Atmos. Sci*., **67**, 3904-3915.

Squires, P., 1956: The microstructure of cumuli in maritime and continental air. Tellus, 8, 443–444.

- - -, 1958: The microstructure and colloidal stability of warm clouds. Part I: The relation between structure and stability. Tellus, 10, 256–261.

Squires P. and S. Twomey, 1960: The relation between cloud droplet spectra and the spectrum of cloud nuclei. *Physics of Precipitation,* Geophys. Monogr. **No. 5**. Washington. D.C., Amer. Geophys. Union. 71 I.

Stephens, G. L., P.J. Webster, R.H. Johnson, R. Engelen and T. L'Ecuyer, 2003: Observational evidence for the mutual regulation of the tropical hydrological cycle and tropical sea surface temperatures. *J. Climate*, **18**, 237-273.

- - -, N.B. Wood and L.A. Pakula, 2004: On the radiative effects of dust on tropical convection. *Geophys. Res. Lett*., **31**, L23112, doi:10.1029/2004GL021342.

- - -, 2005: Cloud feedback in the climate system: A critical review. *J. Climate*, **18**,237-273.

- - -, S. C. van den Heever and L.A. Pakula, 2008: Radiative-convective feedbacks in idealized states of radiative-convective equilibrium. *J. Atmos. Sci*., **65**, 3899-3916.

Takemi, T., O. Hirayama, and C. Liu (2004): Factors responsible for the vertical development of tropical oceanic cumulus convection, *Geophys. Res. Lett.*, **31**, L11109, doi:10.1029/2004GL020225.

Tompkins, A.M., and G.C. Craig, 1998a: Radiative-convective equilibrium in a threedimensionalcloud-ensemble model. *Quart. J. Roy. Meteorol. Soc*., **124**, 2073-2097.

Twomey, S., and J. Warner, 1967: Comparison of measurements of cloud droplets and cloud nuclei. *J. Atmos. Sci.*, **24**, 702-703/

- - -, 1974: Pollution and the planetary albedo. *Atmos. Environ*. **8**, 1251-1256.

- - -, The influence of pollution on the short wave albedo of clouds, *J. Atmos. Sci*., **34**, 1149–1152, 1977.

Twohy, C. H., and M. R. Poellot (2005), Chemical characteristics of ice residual nuclei in anvil cirrus clouds: Implications for ice formation processes, *Atmos. Chem. Phys*., **5,** 2289–2297.

- - -, et al. (2009), Saharan dust particles nucleate droplets in eastern Atlantic clouds, *Geophys. Res. Lett*., **36**, L01807, doi:10.1029/2008GL035846.

van den Heever, S. C., G. L. Stephens, and N. B. Wood, 2011: Aerosol indirect effects on tropical convection characteristics under conditions of radiative-convective equilibrium, *J. Atmos. Sci*., **68**, 699-718.

- - -, G.G. Carrio, W.R. Cotton, P.J. DeMott, and A.J. Prenni, 2006: Impacts of nucleating aerosol on Florida storms. Part I: Mesoscale simulations. *J. Atmos. Sci*., **63**, 1752- 1775.

- - -, W. R. Cotton, 2007: Urban aerosol impacts on downwind convective storms. *J. Appl. Meteor. Climatol*., **46,** 828–850.

Walko, R.L., W.R. Cotton, M.P. Meyers, and J.Y. Harrington, 1995: New RAMS cloud microphysics parameterization. Part I: The single-moment scheme. *Atmos. Res*., **38**, 29-62.

- - -., L.E. Band, J. Baron, T.G.F. Kittel, R. Lammers, T.J. Lee, D. Ojima, R.A. Pielke, C. Taylor, C. Tague, C.J. Tremback, and P.L. Vidale, 2000: Coupled Atmosphere–Biophysics–Hydrology Models for Environmental Modeling. *J. Appl. Meteor*., **39**, 931–944.

Warner, J., and S. Twomey, 1967: The production of cloud nuclei by cane fires and the effect on cloud droplet concentrations. *J. Atmos. Sci*., **24,** 704-706.

Xue, H., and G. Feingold, 2006: large-eddy simulations of trade win cumuli: Investigation of aerosol indirect effects. *J. Atmos. Sci*., **63**, 1605-1622.

Zuidema, P., 1998: On the 600-800 mb minimum in tropical cloudiness. *J. Atmos. Sci*., **55**, 2220-2228.